UNIVERSIDADE D
COIMBRA

Joana Maria Rodrigues Teixeira

Automation of Co-registration of Pre-clinical RPC-PET Images With Animal MRI

Dissertação no âmbito do Mestrado Integrado em Engenharia Física, ramo de Instrumentação, orientada pelo Professor Doutor Paulo Alexandre Vieira Crespo e pelo Professor Doutor Nuno David Sousa Chichorro Fonseca Ferreira apresentada ao Departamento de Física da Faculdade de Ciências e Tecnologia da Universidade de Coimbra.

Setembro de 2019

UNIVERSIDADE D
COIMBRA

Joana Maria Rodrigues Teixeira

AUTOMATION OF CO-REGISTRATION OF PRE-CLINICAL RPC-PET IMAGES WITH ANIMAL MRI

Dissertação no âmbito do Mestrado Integrado em Engenharia Física, ramo de Instrumentação, orientada pelo Professor Doutor Paulo Alexandre Vieira Crespo e pelo Professor Doutor Nuno David Sousa Chichorro Fonseca Ferreira apresentada ao Departamento de Física da Faculdade de Ciências e Tecnologia da Universidade de Coimbra.

Setembro de 2019

This work was developped in collaboration with:

Aos meus avós,
Olímpia e José Luís,
Graça e Acácio.
Foi por vós. Foi para vós.

Acknowledgments

Em primeiro lugar, quero deixar um agradecimento especial aos meus orientadores. Ao Professor Doutor Paulo Crespo, por todo o entusiasmo com que me acolheu neste projecto, por todos os ensinamentos e pela prontidão a responder a todas as minhas dúvidas. Ao Professor Doutor Nuno Ferreira, por toda a ajuda no desenvolvimento do código implementado e toda a disponibilidade na resolução dos problemas que foram surgindo ao longo deste percurso.

Ao Professor Antero Abrunhosa, deixo um agradecimento por me ter permitido integrar neste projecto, colocando à minha disposição os dados de imagiologia pré-clínica adquiridos no ICNAS e sem os quais não seria possível levar a cabo este trabalho.

Ao Doutor José Sereno e à Ana Carolina Xavier, investigadores no ICNAS, agradeço toda a disponibilidade para fazer novas aquisições e toda prontidão e paciência para esclarecer todas as minhas dúvidas, mesmo fora de horas.

Ao Professor Doutor Paulo Fonte, deixo um agradecimento pela integração no grupo de investigação RCP R & D e ao LIP pela disponibilização de todos os meios necessários ao desenvolvimento deste projecto.

Quero ainda deixar um obrigada a toda a minha familia e amigos, que de uma forma ou de outra, tiveram um papel fundamental ao longo de todo o meu percurso académico e do meu crescimento pessoal.

Ao papá e à mamã, agradeço por tornarem tudo isto possível e fácil, por me proporcionarem todos estes anos em Coimbra sem nunca duvidarem de que era capaz. À Catarina, por ser o meu maior modelo de força e de coragem. Às minhas

três madrinhas, a Nela, a Nanda e Guida, pela a preocupação e compreensão constante, por me ensinarem a relativizar e a esperar pelo tempo.

À Bruna, quero agradecer por ser companheira de todas as horas, por aturar o mau humor matinal e a falta de hora de refeições, por todos os apontamentos a meias e todas as horas deste infindável verão. Ao Talisca, agradeço por toda a calma e paciência (e correcções de última hora).

À Filó agradeço a eterna alegria e à Maria Ana o conselho sempre certeiro, às duas agradeço por serem companheiras de viagem e de noites infindáveis de estudo e de copos, vocês são a melhor descendência que alguém pode pedir. Ao Mauro, a paciência e a amizade.

À Rita, ao João Ricardo, ao Rui, ao Ruben e ao Ricardo, deixo um agradecimento mais longínquo, por serem sempre porto de abrigo com uma super numa mão e um abraço na outra. Ao João e ao Francisco, agradeço por serem a minha melhor definição de amigo.

Para todos eles, por todas as lágrimas que limparam, por todos os sorrisos que me deram, por caminharem sempre de mão dada comigo, o meu obrigada vai ser sempre pouco.

Resumo

A imagiologia médica é um dos recursos mais utilizados na medicina, sendo as suas principais aplicações no diagnóstico e terapêutica. Imagens obtidas através da fusão de duas modalidades de imagiologia médica apresentam vantagens consideráveis quando comparadas com images provenientes de uma só técnica de imagem, uma vez que combinam informação anatómica com informação funcional. Enquanto a Tomografia por Emissão de Positrões (PET) fornece informações específicas acerca do metabolismo, estudos de Imagiologia por Ressonância Magnética incluem formas anatómicas com elevado contraste, destacando-se o seu desempenho na distinção de tecidos moles. Desta forma, a combinação das duas técnicas fornece parâmetros funcionais combinados com informação espacial adicional.

Neste projecto, pretendemos desenvolver uma interface gráfica para a automatização do co-registo de imagens obtidas em estudos de RPC-PET pré-clínico com images de MR animal de forma eficiente. A análise dos pacotes de software disponíveis para este propósito foi feita tendo em conta a amplitude de funcionalidades, a extensibilidade, a portabilidade entre plataformas, o tipo de licença e a possibilidade de aplicação em meio clínico. A plataforma de desenvolvimento do *Interactive Data Language* (IDL) destacou-se sobre os seus pares cumprindo todos os requisitos necessários para o desenvolvimento deste projecto.

O desenvolvimento do algoritmo de co-registro teve por base o método de medição de pontos de referência, usando a intensidade e a posição dos centróides dos cinco marcadores fiduciais colocados na cama usada em ambos os equipamentos de aquisição de imagem. A matriz da transformação de registo é determinada pela minimização da métrica de semelhança através de um processo de optimização, e

aplicada ao volume de RCP-PET. Uma interface gráfica interactiva permite a visualização e manipulação dos volumes co-registados.

O algoritmo de fusão foi aplicado a diferentes casos clínicos de imagiologia animal, adquiridos com e sem ratinhos marcados com diferentes radionuclídeos. O desemplenho do programa foi validado qualitativa e quantitativamente, tendo-se obtido um valor médio de TRE (Erro de registo relativamente ao volume alvo) de 1.906 mm. A avaliação das volumes resultantes do processo indica como principal fonte de erro o método de identificação do limiar de intensidade.

Por último, foram feitas algumas considerações relativas a potencias melhorias do método desenvolvido.

Palavras chabe: *MRI animal, RCP-PET pré-clínico, Imagiologia Multimodal, Co-registo de Imagem, Imagiologia Animal*

Abstract

Medical imaging is one of the most common resources in medicine, where the main applications are within disease diagnosis and monitoring of treatment. Images obtained resorting to two different procedures of medical imaging show considerable advantages when compared with single methods, as both anatomical and functional information are provided with more accuracy. While positron emission tomography (PET) provides a specific metabolic signal, magnetic resonance imaging (MRI) includes anatomical information with superior soft-tissue contrast: the combination of the two methods provides functional parameters and additional spatial information.

In this work, we aim at developing a graphical interface for automating the co-registration of images obtained through a pre-clinical RPC-PET system and its image fusion with an animal magnetic resonance system efficiently. Software comparisons were performed considering the breadth of functionality, extensibility, cross-platform portability, and non-restrictive software license, as well as future applicability in clinical settings. It was considered that the Interactive Data Language (IDL) software development package is the one that best fits the current project.

The co-registration algorithm is based on the landmarks measurements method grounded on the pixel intensity and the location of the centroids of the five artificial fiducial markers placed on the examination bed used on the two acquisition equipment. The registration transformation is determined by the minimization of the feature-based metrics. After this optimization process, the source image (RCP-PET) is transformed and interpolated. The merged volumes are displayed in a GUI that allows basic volume manipulation steps.

The performance of the co-registration was evaluated by testing the algorithm in different datasets acquired with and without small animals (mice) labeled with several radionuclides. The registration results were qualitative and quantitative validated and for the 19 studies successfully merged the mean value for TRE (Target Registration Error) was 1.906 mm. The results obtained suggest that the major error source is related to the fiducial markers and the routine for threshold identification. Finally, considerations on potential improvements to the method are made.

Keywords: *Small Animal MRI, Pre-clinical RCP-PET, Multimodality Imaging, Imaging Co-registration, Small Animal Imaging*

Acronyms

AMIDE Amide's Medical Image Data Examiner.

CAD Computer-Aided Design.

CT Computed Tomography.

DICOM Digital Imaging and Communications in Medicine.

FOV Field of View.

GUI Graphical User Interface.

IDL Interactive Data Language.

MI Mutual Information.

MR Magnetic Resonance.

MRI Magnetic Resonance Imaging.

OS Operative System.

PET Positron Emission Tomography.

PMT Photomultiplier tubes.

RF Radiofrequency.

RIU Ratio of Image Uniformity.

RPC Resistive Plate Chamber.

SI Source Image.

SPECT Single Photon Emission Computed Tomography.

TI Target Image.

TRE Target Registration Error.

List of Figures

List of Tables

Contents

1

Introduction

This chapter intends to present a context to the problem that brought up this dissertation. We present the motivation, and goals of the project. Finally an explanation of the structure of this document is present.

1.1 Context

This document was carried out as part of the Project discipline, during the academic year of 2018/2019. It corresponds to a dissertation to be submitted to the *Faculdade de Ciências e Tecnologias da Universidade de Coimbra* (FCTUC) in fulfillment of the requirements to obtain the Master Degree in Physics Engineering.

This project emerged as part of the RPC R&D research line of the *Laboratório de Instrumentação e Física Experimental de Partículas* (LIP) in partnership with (FCTUC) and *Instituto de Ciências Nucleares Aplicadas à Saúde* (ICNAS).

1.2 Objectives

The automation of the co-registration of pre-clinical RPC-PET images with small animal MRI was the main goal of this project.

To achieve such purpose, a few tasks were considered. First the state of the art review, regarding methodologies for multimodality image registration, was made. The next step was the acquisition of the RPC-PET and MRI studies and the analysis

of the features of the data. In the next stage software platforms available for the development of the registration interface was tested and analyzed. After the co-registration algorithm was developed and the GUI for visualization of the merged volumes was adapted. Finally, the co-registration algorithm was implemented to the acquired data sets and the results was evaluated.

1.3 Structure

This dissertation is organized in five main chapters.

Chapter 2: Theory provides a background on stand-alone medical imaging modalities emphasizing PET and MR imaging. Moreover, an insight into multimodality imaging is presented. The image registration techniques are also reviewed in this chapter. Finally, the state-of-the-art subsection summarizes previous research on image registration techniques pointing the main results..

Chapter 3: Methods describes the methodology used to design the co-registration system from the medical image acquisition until the visualization of the merged volumes.

Chapter 4: Results presents the performances achieved with the implementation of the co-registration algorithm.

Chapter 5: Discussion and Conclusions evaluates the results of the work, comparing them to its objectives. Finally future work possibilities are highlighted.

2

Theory

Throughout the next sections, a theoretical outline of the medical imaging techniques is presented, and the techniques handled during this project, as well as the advantages and disadvantages of combined Positron Emission Tomography (PET)/Magnetic Resonance Imaging (MRI) techniques are emphasized. Image Registration techniques are also explained. Finally, research developed on co-registration algorithms is summarized.

2.1 Medical Imaging Modalities

Medical Imaging comprises a set of different non-invasive techniques and methods, used to create a representation of the interior of the body for clinical purposes. In the field of medical imaging, different acquisition technologies lead to different types of images. Each one of them gives distinct information about the subject being studied.

Therefore, we can acknowledge Medical Imaging as a reliable way to represent anatomical structures of the body by using various techniques such as X-Ray Computed Tomography (CT), MRI or nuclear medicine techniques [8]. Figure 2.1 shows the major diagnostic imaging categories, and the most frequent assistant techniques are presented.

Based on the assumptions that each diagnostic technique uses a particular technology, we can conclude that each one produces different output images. The information from these images can be used separately, or by combining it with

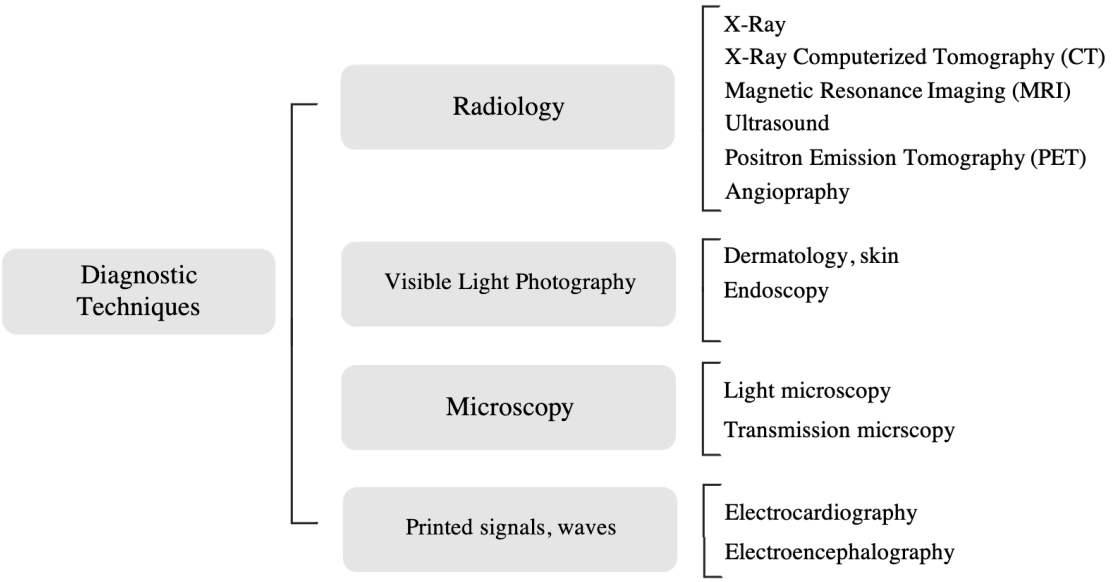

Figure 2.1: Diagnostic techniques resume scheme. The four major areas of diagnostic imaging techniques are presented. Based on [1]

other medical data. Table 2.1 compiles the most frequently used radiology techniques, and their features.

Computerized Tomography (CT) uses X-rays to produce a series of cross-sectional images of the body that are reconstructed by a computer. Its main advantages are the wide Field of View (FOV) the high spatial resolution, and the high penetration depth. Detection of subtle differences in the analyzed tissues is possible, yet the soft tissue contrast is poor and each examination yields a high radiation dose to the subject [9].

At the same time, Magnetic Resonance Imaging (MRI) also produces anatomic representations of the body. However, this technique uses magnetic signals instead of ionizing radiation. MRI presents higher spatial resolution and a remarkable capability to show anatomical details. The main disadvantage of this technique is the magnetic field disturbances that cause field inhomogeneity, and its superior cost [6].

Nuclear medicine modalities - Single Photon Emission Computed Tomography (SPECT) and PET - have as main purpose the detection of the isotope distribution within the body tissues of the subject [9]. Whereas SPECT uses radioisotopes that decay emitting a single gamma photon, PET applies

Table 2.1: A comparison of the most frequent assistant radiology imaging techniques. Brief summary of their main characteristic, contrast, applications, cost, and radiation type. Adapted from [6].

	CT	MRI	PET	SPECT	Ultrasound
Main Characteristic	Scan body organs using X-rays and produce a series of cross-sectional based images via the computer	Produce "slices" that represents the human body through applying magnetic signals	Nuclear imaging technique example where the tracers are used in diseases diagnosis	A non-invasive based technique where cross-sectional images of radiotracer within the human body are structured	Sound wave based technique capable of producing quantitative and qualitative diagnostic information through a set of comprised methodologies
Contrast	High	High	-	-	-
Application	Anatomical	Anatomical	Functional	Functional	Anatomical
	Functional	Functional	Metabolic	Metabolic	Functional
		Molecular	Molecular		
Cost	Intermediate cost	Intermediate cost	High cost	Intermediate cost	Low cost
Radiation Source Type	X-Rays (ionizing)	Electric Magnetic Fields (non-ionizing)	Positrons and gamma radiation (ionizing)	Gamma rays (ionizing)	Sound waves (non-ionizing)

radioisotopes that produce a pair of photons in each annihilation process [8]. Although both techniques present some disadvantages (such as limited spatial resolution, the use of ionizing radiation, and the cost) their high penetration depth and sensitivity stands out. Images obtained with nuclear medicine often detect the presence of abnormalities with high contrast, but with less anatomical detail. To overcome for these limitations, co-registration of PET images with CT or MR

images are often used as a complement.

Finally, ultrasound imaging is a technique based on sound waves with no use of ionizing radiation. It resorts to a high temporal frequency to produce quantitative and qualitative diagnostic information. It also presents high axial resolution and a radiation free profile at a low cost. On the other hand, this modality presents limited resolution due to attenuation phenomena [9].

Medical imaging is one of the most powerful medical resources available used all over the world for both diagnosis, and therapeutic purposes. A compromise between power and radiation dose must be made in order to guarantee patient safety without losing important information. Moreover, the current need to efficiently store and retrieve images in clinical applications has become a compelling necessity in the computer field [10].

In this essay, we focused on PET and MR small animal images and on the images obtained by combining the two.

2.1.1 Positron Emission Tomography

PET is a type of computed tomography which uses positron-emitting nuclides distribution in patients to form images. As said above, radioactive substances are administered to the patient. These radioactive isotopes decay producing a positronwhich is combined with an electron of the tissue. The interaction between the positron and the electron will then be responsible for the conversion of both their masses into annihilation radiation, described in detail in Fig. 2.2. This process produces two photons that are emitted simultaneously in almost opposite directions - gamma-ray emission.

Conventional PET systems are composed by several rings of detectors - surrounding the patient - and a circuit which identify the pairs of photons coming from the annihilation processes trough coincident event detection. The obtained projections of the activity distribution are then analyzed and processed in the computer of the PET system and reconstructions of transverse images from the projection data are built [8].

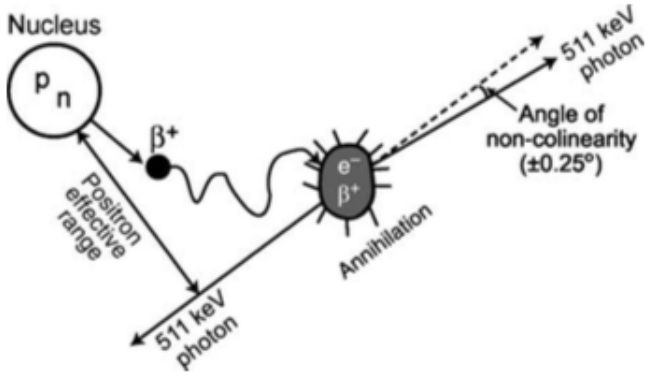

Figure 2.2: Positrons travel a distance before annihilation, the absorber and the distance increases with the positron energy. While positrons with different energies travel in zigzag directions, the effective range is the shortest distance between the nucleus and the direction of 511 keV photons. This effective range degrades the spatial resolution of the positron scanner. [2].

The contrast in PET scans is proportional to the tissue's capability to concentrate the radioactive, but it also depends on several factors, such as: scattered radiation, size of the lesion and patient motion. The radiotracer concentration in a given tissue relates to the administered dosage of the tracer and to the absorption in the tissue [2]. We should remember that the uptake time of the radiopharmaceutical depends on the pathophysiology of the tissue in study. Cardiac and respiratory function may lead to image artifact that also could reduce the image quality.

As well as the image contrast, the spacial resolution should be considered in the image quality evaluation. The spatial resolution of a PET system is mainly limited by the intrinsic resolution of each detector, the distance travelled by the positrons before annihilation, and the fact that photons emitted in the annihilation process are at 180 degrees from each other. Another critical factor is the organ motion. As referred before, it affects the image contrast and also plays an important role in the quality evaluation of the spatial resolution.

PET images have major application in oncology - often scans of cancer patients allow understanding the disease extension and give support during the treatments. However, PET imaging has limitations - they show the abnormalities with high contrast but poor anatomic detail. As an attempt to solve this, PET images are usually co-registered with CT or MRI images which present better outcoming in anatomical descriptions.

2.1.2 Magnetic Resonance Imaging

The biological tissues of the body have a high abundance of hydrogen atoms, which have nuclear magnetic resonance properties - magnetic momentum, the ability to precess about its axis and to absorb radio wave energy at high frequency when under a magnetic field of the order of 1.5 T [8] . The MRI image technique uses maps that are characteristics of the tissue and then creates anatomical images of the bodies in study.

In MRI examination, the patient lies on the magnetic field with the coils placed around. The antennas produce a pulse of radio waves which is absorbed by the protons in the tissues and subsequently reemitted by them. The coils placed around the patient also detect the radio wave emitted by the protons. As frequency is proportional to magnetic field strength, using magnetic field gradients (changes in the strength of the magnetic field as function of the body of the patient), the proton resonance frequency will vary as function of position. Therefore, on MRI systems the frequency of the returning radio waves allow us to know the location of each signal and then reconstruct the images.

Images produce by MRI systems demonstrate high sensitivity to anatomical variations and high contrast due to different local magnetic properties of the tissues. Each point in an image represents a point of the tissue area under study, its appearance on the images depends on their micromagnetic properties [11]. MRI produces a set of tomographic images describing slices through the body of the subject. Scans could be made using different data acquisition methods, and acquisition pulse sequence could offer high-quality images with selectable tissue contrast.

2.2 Combined PET/MRI

As mentioned before, imaging modalities present both limitations and advantages. To minimize these weaknesses, medical imaging is changing from stand-alone techniques towards multimodal imaging. Different modalities are combined to

reach both functional and anatomical information in just one image.

Nowadays, nearly all PET systems manufactured are coupled to x-ray CT systems - a single bed passes through the bores of both systems. PET/CT systems have substantial limitations: the data acquisitions are not simultaneous, and there is an additional contribution of radiation dose by CT.

An alternative to the PET/CT systems are dual modal PET/MRI systems. Functional PET information is co-registered with anatomical MRI data, as shown in Fig. 2.3. To achieve dual modality images, two approaches have been developed - acquisition on PET/MRI scanners and software-based image co-registration of images from independent PET and MRI scanners.

In the following subsections, these two approaches will be categorically explained.

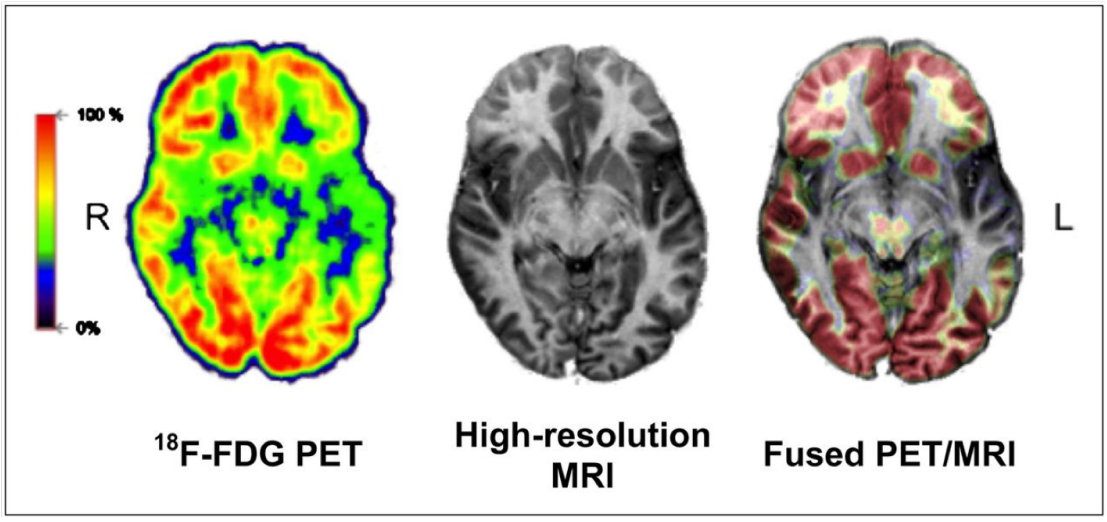

Figure 2.3: Simultaneous PET/MRI study. From left to right axial FDG-PET, high-resolution MRI scan and fusion image can be observed [3].

2.2.1 Hybrid PET/MRI Systems

Both PET and MRI are advanced imaging technologies. Nevertheless, a major goal is to combine these two techniques without signal distortion, and without degrading the original performance of each modality. Furthermore the main challenge of merging the two imaging techniques into a single system is the space constraints and the use of Photomultiplier tubes (PMT) at PET detectors which

do not operate properly in the presence of magnetic fields [12].

There are three possible ways of combining the two systems. The first and simplest, is to place the two scanners in series analogous to the current PET/MRI systems. However, as the PET detector is affected by the magnetic field, it is necessary to adapt it in a way that it is no longer affected by the MRI system.

The best way to solve these problems is to fully integrate the two systems in such a way that PET hardware is coupled into the MRI gantry. Neverthless, the same problem is imposed - the mutual interference between the two systems, which could compromise the success of the whole system. The strong static magnetic field of the Magnetic Resonance (MR) scanner interferes with the PET, Radiofrequency (RF) interferences and induced currents, from the switching of the gradient system may occur as well. On the other hand, putting the PET system inside the MR device could cause distortion of the main uniform magnetic field of the MR system. The attenuation correction is also an obstacle.

With the main goal of achieving a combined system that overcomes the technological problems, several prototypes have been under development over the last few years. To solve the PMT sensitivity problem, several different technical approaches have been studied, such as *Long Light Fiber PET/MR systems*, *Slip Magnet PET/MRI systems*, *PET/MR Systems that Couple the Light Detectors Directly to the Scintillation Crystals*, among others [13]. Recently, the use of silicon photomultipliers and avalanche photodiodes as photon detector technology in PET/MRI technology allowing whole-body simultaneous PET/MRI are already approved for clinical us [14]. A

Despite being an expensive technology, fully integrated PET/MRI systems have considerable potential in imaging applications, allowing the correlation of functional and anatomic images, and the simultaneous acquisition of multifunctional data, such as PET tracer uptake or MR spectroscopy.

2.2.2 Software-based PET/MRI Image Co-registration

Another approach to obtain dual modality images is a software-based solution for PET/MRI co-registration. Data acquired in medical services from separated imaging systems are used to transform images of both modalities to match through manual or automatic software algorithms [15].

In software-based co-registration we superimpose PET images to MR images. Tipically, the PET outputs are the source images, and these are the ones getting altered throughout the fusion process. The MR outputs are the target images, and those remain unchanged during the process.

Usually, the co-registration algorithms base themselves on known anatomical structures (anatomical landmarks) or on fiducial markers (artificial landmarks) and these algorithms are known as featured based algorithms. This is an approach usually used in manual co-registration. Alternatively, automatic software often uses voxel intensity as a reference [11].

The major problem of this technique relates to the fact that image acquisition is not simultaneous. As we obtain the images from different scanners, it is quite difficult to achieve the same patient's position during the two acquisitions. This leads to the presence of artifacts in the images that interferes with the accurate image co-registration [11].

PET/MRI systems offer advantages that cannot be sufficiently achieved in software-based techniques. Nevertheless, the capital investment required for initial purchase and infrastructures upgrades makes this software-based solution worth it [15]. With this work we intend to create a software-based solution that accomplishes the benefits of integrated PET/MRI animal scanners.

2.3 Image Registration

Imaging modalities presents limitations, which can be overcome by combining different modalities to reach both functional and anatomical information. Medical

image registration is the process of intelligently aligning two or more images into a single one that provides more information for decision making. The process of image registration is also known in the literature as image superimposition, matching or merge [16]. Registration procedures are based on the definition of transformation in which one image (source image) is specially adjusted (translated, scaled, rotated, and deformed) relative to another fixed image (target image).

The information from different images that can be accurately related using a software approach is a demanding process. Major issues related to multimodality imaging concern problems related to the file structure and its manipulation, the registration methods itself and, storage and visualization of the merged images [16].

An image registration process requires making a certain number of decisions and processing steps in order to determine spatial correspondences. Firstly, the choice of the transformation and the measure of alignment are made. Then, the target and the source images are selected and the pre-processing to delineate correspondent structures is made. The computation of the transformation is made by the optimization of the measure of alignment. The transformation of the source image to the coordinate system of the target image is finally obtained. As last, the results are shown and the user can manipulate them [17].

Image registration methods can be applied to images of the same subject - *intra-subject* co-registration - or images of different subjects - *inter-subjects* co-registration. Besides, correspondences can be established between images obtained from the same imaging modality or from different imaging modalities. [17]. The first one is usually made using images obtained in different time-frames and helps to correct motion artifacts due to cardiac or respiratory motion. The last one uses images from different modalities and allows to correlate different views of the structure under study [18]. Fig. 2.4 classifies the different image resgistration applications.

With regard to intra-subject registration we have four applications: multimodality registration, correcting PET emission data, serial image registration and registration of images to physical space. Multimodality registration concerns the combination of a couple of medical images of the same structure off a subject obtained with different

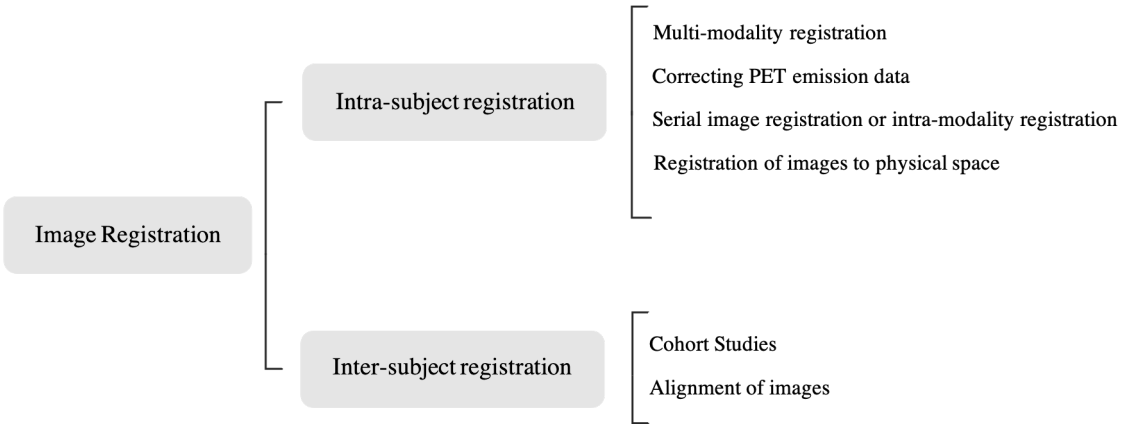

Figure 2.4: Scheme of classification of medical image registration applications.

imaging modalities in order to reveal complementary information. It is usually used to accomplish a relation between functional and anatomical information and it is commonly achieved by the combination of PET or SPECT images with CT or MR images.

In its turn, correcting PET emission data is used to improve the accuracy of regional uptake, make photon attenuation corrections or improve co-registration accuracy. Corrections are made with information obtained by aligning anatomical images or using CT attenuation maps.

Serial image registration or intra-modality registration uses images taken over time with the same imaging techniques. This intents to monitor minor changes in the images and correct artifacts due to the motion of the subject over the examination.

Regarding to registration of images to physical space, we have that is used in interventional, surgical, or therapeutic technologies to guide specific treatments. That technique forces that the information derived from the registration be continuously aligned with physical space during treatment [17].

At last, inter-subject registration might be related with cohort studies and with image alignment. In cohort studies, images from a group or cohort are aligned to improve sensitivity. On its turn, image alignment concerns to the process of superimposing images to an anatomical atlas to help to recognize specific anatomic structures [17].

Medical image registration could also be separated into extrinsic and intrinsic

methods. The first ones are based on foreign objects introduced into the image space and the second ones are based on the image information produced by the patient himself [19].

Even though all registration applications play an important role in the medical plane, from now on we are just focusing on intra-subject multi-modality registration.

2.4 Registration Techniques

Multi-modality registration algorithms focus on accurate aligning a set of medical images generated using different acquisition techniques. Considering a software approach, merge functions should find correspondence between the images and provide useful visual information by superimposing a couple of images from different modalities [20].

In general, such data from different modalities presents an inevitable misalignment due to the different dimensions of the images. Finding the association between intensity values of analogous pixels is another challenge. On top of that, also the high variability of tissue appearance under different modalities becomes an issue [4].

The fusion algorithms can either be based on rigid or nonrigid transformations. When the co-registration lays on rigid transformations of the PET image, it merely undergoes translation, rotation, scaling and/or shear movement comparatively to the MRI image. In this type of transformation the relation between distance, lines and angles are preserved. On the other hand, when nonrigid transformations are also applied affine transformation, similarity transformation and/or perspective projection also could be made. The shape of the source image may be altered causing distortion and errors on the final image [11, 6]. Equation 2.1 mathematically emphasize these transformation with up to four parameters w_{xy}, where x and y are the coordinates of the target image .and x'

and y' are the coordinates of the source image after the transformation.

$$\begin{bmatrix} x' \\ y' \\ 1 \end{bmatrix} = \begin{bmatrix} w_{11} & w_{12} & 0 \\ w_{21} & w_{22} & 0 \\ 0 & 0 & 1 \end{bmatrix} \begin{bmatrix} x \\ y \\ 1 \end{bmatrix} \tag{2.1}$$

Image algorithms can also be distinguished from those that use landmark or surface and edge mesures and those that use voxel intensity measurements to find the geometrical transformation between the Source Image (SI) and the Target Image (TI). Figure 2.5 illustrate the registration process, where the source image is transformed to target image according to Equation 2.2.

$$T = arg_T max SM(T(SI(x, y, z)), TI(x, y, z)) \tag{2.2}$$

Registration algorithm is accomplish by finding the registration transformation (T) that best aligns the images in accordance with the choice of the similarity measurement [17]. The features of the source image are then mapped into the analogous target image space by the transformation function. As a result, source image coordinates are transformed to the corresponding target image coordinates.

Transformations based on similarity measurements are a particular case of the affine transformations. As angles between lines are not affected by the change of the lines and positions of points, the shapes of the imaging objects are preserved. Assuming that the method only takes into account translation, rotation, and uniform scaling, the three dimensional similarity transformation depends on three translation and three rotation parameters, and on one scaling factor [21].

The most common errors in the co-registration process, which propagates along the process, are due to the sample size, imperfections of the acquisition system used, noise or interpolation methods used. The cost function also may lead to misregistration.

Choosing the similarity measure is a head step in the fusion algorithm design. According to [11, 17] the similarity measurements can be divided into three

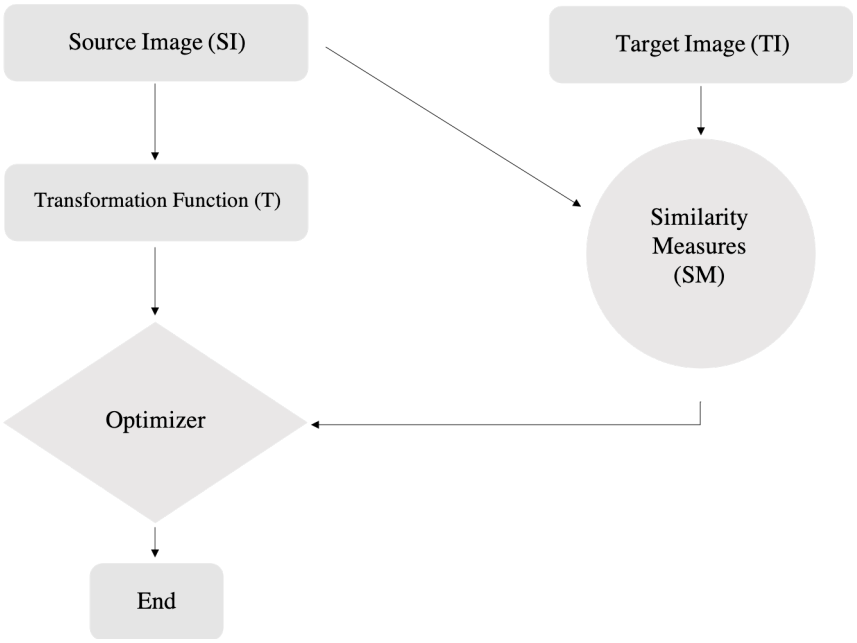

Figure 2.5: Similarity measure process scheme. Adapted from [4]

different categories - landmark measurements, surface and edge measurements, and voxel intensity measurements - as summarized on Table 2.2 and it will be explained further on.

2.4.1 Landmark Measurements

Landmark measurements, also treated on literature as corresponding point [17] - are one of the earliest methods used to successfully co-register a couple of medical images. The method uses anatomic features or external markers that are visible in two images to be co-registered as control points. External markers are attached in a specific place on the examination bed, settling a relationship between the structures that are being imaged [22].

Since the subject constantly moves due to cardiac and respiratory motion, consistently placing the markers on the same location is a challenging requirement. It is mandatory that the fiducial markers are placed in such a way that minimize the probability that patient movements obstruct the landmarks or move them. It is also important to notice that constraints in the size of the Field of View (FOV) of the imaging device might diminish the choice of fiducial markers. At last, in the

Table 2.2: Comparison of registration methods based on similarity measurements for medical images using accuracy, efficiency, reliability and transformation as evaluation parameters. Based on [7].

	Landmark measurements	Surface and Edge Measure	Voxel Intensity Measure
Accuracy	Accuracy depends on precise correspondence between landmarks and on the accurate localization of a sufficient number of correspondent landmarks	High accuracy when the pre-processing segmentation step is performed precisely	Accuracy strongly dependent on the intensity variations
Efficiency	High processing time	High efficiency when registered structures are clearly visible and easy to segment.	High, because it can directly operate on image gray values and does not require preprocessing and user interaction
Transformation	Non-rigid/rigid and low dimensional; Good feature alignment Faster to compute the mapping transformation then surface based or intensity based registration.	Allows rigid and non-rigid transformations	Rigid, non-rigid and global transformations

case of multimodality registration, markers properties must make them distinguishable on both imaging modalities. Using external markers instead of anatomic features has the main advantage of providing absolute reference points in both images [11, 23].

Image transformation is defined by mapping the landmarks location in the first image onto their location in the second image using a mean square error. When internal

anatomic landmarks are used, co-registration processes require considerable operator expertise, however the use of external landmarks usually leads to fast registration [16].

Processing using landmark measurements provide alignment enough to make this method a "gold standard" agains other registration methods [23].

2.4.2 Surface and Edge Measurements

Surface and edge measurements registration method has been usually implemented with images that have net contours [16]. This technique attempts to use features provided by the boundaries or surfaces between organs and between the skin surface and the surrounding air for image registration. Automatic or user-defined segmentation is used to define boundaries of surfaces or edges in the images to be co-registered. When these surfaces or edges correspond to the same structure in both images then they are used to derive the registration transformation. In summary, this approach attempts to minimize the distance between the surfaces and edges previously identified and segmented [24, 11].

This technique was initially proposed to align MRI, CT and PET images of the head due the symmetry of the structures under study [11]. Since then the method was adapted to images of different parts of the body, however still usually only used to design rigid body transformations [17].

Surface and edge detection techniques match images by minimizing the mean square error on distance between the surfaces visible and comparing intensity values of the pixels identified as part of the contours on both modalities. The use of this technique in medical imaging applications is considered because in most cases the edge information is the only feature that the images have in common. The implementation of this technique requires user expertise about singularities of the images [25].

2.4.3 Voxel Intensity Measurements

Voxel intensity measurements technique is based on the direct analysis and manipulation on voxel intensities. Image alignment is measured directly from the voxel intensities and the transformation that maximizes this measure is searched by an optimization process. Since medical images have high-resolution, optimization process might be a demanding operation requiring a high number of computations. Great computational power is then essential for quickly handle and co-registered medical images [17].

Depending on the modalities of the images that are under study, a number of measurements can be made. According to [26] the sum of the absolute or square intensity measurements difference between a pair of images could be minimized assuming that images differ only by noise. This technique is known as minimization of intensity difference and is usually applied for intra-modality co-registration. Correlation of voxel intensities also stands out for intra-modality fusion algorithms and assumes that a couple of images are strongly correlated [11].

The first approach used is minimum variance measurements technique. The method was firstly applied to images acquired with the same technique and uses the Ratio of Image Uniformity (RIU) algorithm to find the transformation that minimizes the standard deviation of the ratio of the intensity of the images [27, 17]. The second approach of the method was developed for serial PET and MRI studies assuming that voxels with identical MRI signal intensity correspond to a specific tissue type and thus have the same PET signal. The best transformation is obtained by the minimization of the variance of the voxel intensity for each type of tissue [11, 28]. Both approaches computed the ratio on a voxel-by-voxel basis from the target image and the transformed source image.

2.4.4 State-of-the-Art

Over the last few decades, several efforts were made in order to design medical image registration algorithms. In the following paragraphs, a literature review on those methods is made.

In 1989, *Pelizzari et al.* [24] developed a surface matching technique to register multiple tridimensional image scans of the brain that imposes no requirements on scans. Image correlation is based on computer matching surfaces, the surface of anatomical structures that are common in the two images is used to define a specific coordinate reference and the transformation is then applied. The algorithm was tested in CT, MRI and PET images and three-dimensional accuracy on the order of 1-2 image pixels.

In 1992, *Woods et al.* [27] designed an algorithm that calculates the ratio voxel-by-voxel of one image to the other. The method was developed for PET and moves the images relative to one another iteratively in order to find the position that minimize this ratio across the voxel. The validation was made using a 3D humand brain phantom and the maximum misregistration obtained was less than 1.745 mm - the size of a pixel. Later, in 1993, *Woods et al.* [28] modified their previously method to allow intra-subject multimodal co-registration. In this technique the standard deviation of the PET pixel values that correspond to each MRI pixel value is minimized in order to achieve the alignment. Validation was made using data acquired with different patients and a maximal three-dimensional error of less than 3 mm was obtained.

Also in 1992, *Mandava et al.* [29] attempted to register arbitrarily oriented, multimodal, volumes images of the human head with other images and with physical space. Three or more fiducial markers that are attached to the heads under study are used to design the matching algorithm. A one-to-one mapping was made in order to relate information given by both images and to deduced relationships between images and anatomy. This method stands out for trying to register images acquired in any orientation and using any imaging modality. *Wang et al.* [30, 31] later works attempted to improve the fiducial markers, both in shape and material.

In 1994, *Pietrzyk et al.* [25] developed a highly interactive method for multimodality registration in which the accuracy of coregistration is visually examined. As the method is based on edge and surface measurements, their results are highly dependent on image resolution, translation distances, and rotation angles. However, an average displacement of 0.43 and 0.29 mm for PET and MRI

data, respectively, was achieved.

In 1997 *Maurer et al.* [22] efforts aimed to apply landmark measurements in co-registration algorithms. Multimodal image-to-image and image-to-physical registration was tested using CT and MR images and a 1.4 mm registration error was obtained. Geometrical distortion in the images, movement of the patient with respect to the system, and movement of the brain between scanning and surgery was pointed as the error source. Regarding to transformations based on fiducial landmarks, it must be noticed that registrations methods are computationally efficient and easily automated [32]. First approaches to design and use external markers are made at [33, 34, 35].

In 2003, *Rohr et. al* [36] integrated geometric information as additional knowledge to define landmarks by analyzing how voxel intensity varies across an image.

In 2006 *Periaswamy et al.* [37] built up a general volume co-registration method based corresponding points - landmarks [38], edges [39, 40] or features [41, 25] between the pair of the images . The transformations applied to a couple of images are modeled as locally affine but globally smooth taking into account variation in images intensities.

Mutual Information (MI) [42] methods have been extensively used for inter-modality registration based on intensity measurements. Despite being a robust, reliable, and fully automated technique, it has a set of weakness such as slow accuracy and sensitivity. In order to solve the shortcomings of this method, in 2012 *Wachinger et al.* [43] develop a new algorithm based on similar internal structures common in images acquired from different modalities, they also compared the performance of entropy and manifold learning-based methods.

In 2016, *Robertson et al.* [15] proposed a fully automated method to three dimensional images using a deformable image registration technique. Most recently, in 2017, *Brock et. al* [44] presented an overview over the use of registration and fusion algorithms and techniques. A comparison of different algorithms for medical image registration of whole-body MRI was also made by *Ceranka et al.* [45] in 2018.

The registration algorithms mentioned above are widely applied in human registration. However, there is no information about their performance when applied to small animal images and then no guarantee that an accurate registration could be achieved. Small animal images have high anisotropy in voxel dimension due to its very fine bi-dimensional resolution but large slice thickness when compared to images acquired in humans. Furthermore, there is an absence of anatomical details in small animal images. *Vaquero et. al* [46] investigate the possibility of accurate use validated human registration algorithms to small-animal imaging using automated image registration (AIR) algorithm [28], and the mutual information algorithm (MI)[42]. They concluded that MI method is more robust for PET, CT and MR images of the rat head yielding to smaller registration error. AIR algorithm requires excessive user intervention or fail.

Also in 2000, *Hayakawa et al.* [47] based on previous work of *Ardekani et al.* [48] developed a PET-MRI registration technique applied to rat brain achieving satisfactory and useful registration.

Recently, in 2018, *Bricq S et al* [49] proposed an automatic registration tool for preclinical PET/MRI based in non-linear intensity transformation and B-splines, achieving an average error of 0.72 mm. *Bashiri et al.* [20] performed a literature review in both multi-modality and mono-modality registration methods.

In 2019, a review across manual, automatic and landmark registration was to improve liver lesion characterization [50] and a study on the reproducibility and comparability of preclinical PET imaging data in small animal studies was performed by *Mannheim et. al* [51].

3

Methods

In the first section, acquisition modalities and main features of the volumes under analysis are presented, with an assessment to the fiducial markers used. The next step was the analysis and test of the software available for the development of the registration method, in section 3.2.

In the section 3, the methodology developed to the automation of the RPC-PET/MRI co-registration algorithm. The latter was divided in two main stages: a registration stages where the landmarks are identified, the parameters of the transformation are computed and the data interpolation is made, and a visualization stage, which accomplishes the visualization tool for the merged volumes. Finally, the studies carried out to validate the system and their evaluation performance are described.

3.1 Data acquisition

Small-animal *in vivo* imaging is an established and widely used tool in preclinical biomedical research imaging of small laboratory animals (mice and rats). In particular, small-animal MRI merged with small-animal PET (mice) provides a noninvasive way to study biological structure and function *in vivo*, and to collect quantitative, spatial and temporal information on normal and abnormal tissues [52, 11].

In this work, the images under analysis are obtained with and without small animals labeled with several radionuclides under study at the *Instituto de Ciências Nucleares*

Aplicadas à Saúde (ICNAS) in Coimbra. Fiducial markers placed on bed used on both examinations allow the co-registration of images of the two modalities, as highlighted in figure 3.1.

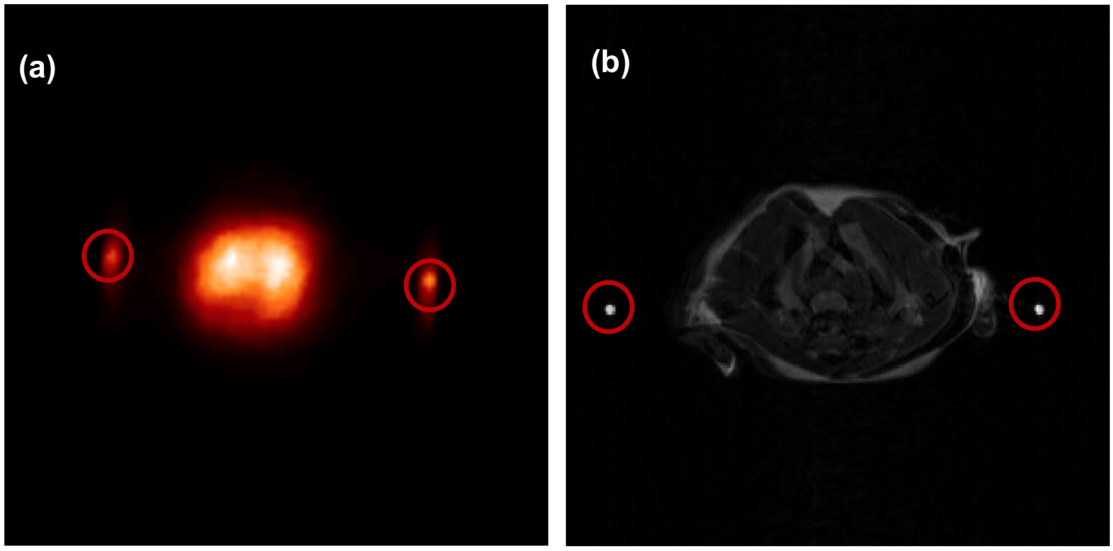

Figure 3.1: Transaxial view of the images in study obtained with mice. RPC-PET image (a) and MRI image (b). The MRI image was obtained with a T2 sequence using long repetition time. In both images, two of the five artificial fiducial landmarkers are identified by red circles.

PET images are acquired in a RPC-Based Preclinical PET prototype [5]. In this device, the converter-plane gamma detection principle is used to apply timing RPCs to PET systems. The whole system is fabricated on the base of four detector heads with 10 RPC-based detectors with 5 gas gaps each. The system is defined with a rectangular cross-section with an area of 35 mm $\times$ 25 mm and a longitudinal length of 160 mm. The Computer-Aided Design (CAD) scheme of the prototype is presented in Figure 3.2. The use of RCP-based detectors offer better time and intrinsic position resolutions with a simple and economic detector construction [53, 54].

The MRI acquisitions are performed with the imaging device *Bruker BioSpin MRI GmbH*[1], which have routines optimized for small rodents. Its architecture is also adapted for preclinical applications, having a 16 cm clear bore size with 72 mm free access for the animal. The device works with fields strengths from 4.7 to 7T and their actively shielded gradient system allow easy and cost-efficient siting. This MRI scan

[1]https://www.bruker.com/products/mr/preclinical-mri.html

provides several acquisition protocols and scanning sequences. The images under study are acquired with T2-weighted protocols, to achieve higher contrast between structures.

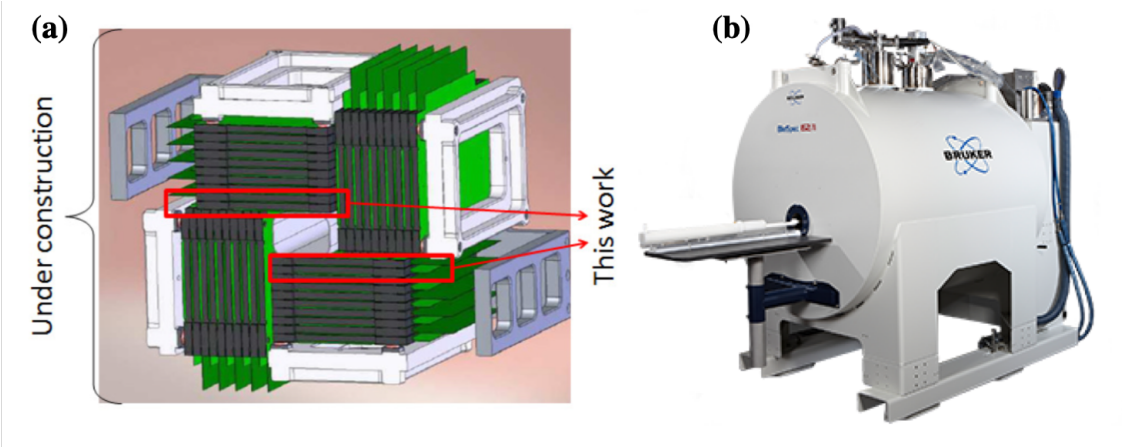

Figure 3.2: Image acquisition equipament. CAD scheme showing the full small-animal RPC-PET prototype in use [5] (a) and Bruker BioSpin MRI GmbH (b).

While MR images are acquired and reconstructed with ParaVision software, RCP-PET images are collected by a Graphical User Interface (GUI) built in Matlab. To follow the standard protocols of treatment, storage, and transmission of medical data, both are stored in Digital Imaging and Communications in Medicine (DICOM), the standard format for medical information. This storage format allows the information to be available in different types of equipment and consoles, as well as at process computers running in distinct Operative System (OS).

Notice that images from different acquisition systems and modalities have different characteristics. Table 3.1 presents images parameters of most interest regarding the desired application of this project. Small animal RPC-PET and MRI have different size and pixel spacing, parameters that have to be taken in consideration in the co-registration process.

3.1.1 Fiducial Markers

The fiducial markers for each acquisition series using a cylindrical tube containing usually a solution with FDG, which is visible in both modalities.

Table 3.1: Main characteristics of the images in study. The images are acquired in DICOM format in order to follow the standard protocol for medical information treatment, storage and transmission. The difference in pixel spacing is one of the main challenges in the co-registration process.

	RPC-PET	MRI
Format	DICOM	DICOM
Width (pixels)	160	256
Height (pixels)	160	256
Slice Thickness (mm)	0.500	0.500
Number of Slices	160	36
Voxel size (mm)	[0.500; 0.500;0.500]	[0.1758; 0.1758;0.500]
Largest ImagePixelValue[2]	65535	11039

In this project, the markers used are filled with a solution with a radioactivity concentration of 1.0 mCi FDG/mL (in water). As the dilution is performed before each acquisition study, may occur fluctuations in its radioactivity concentration between studies.

In order to achieve subvoxel precision, the cylindrical markers' volume must be much larger than the voxel sizes [22]. Dimensions of each fiducial marker are about 1 cm height and 0.8 mm inner diameter. As they are hand-made and placed in the bore for each acquisition series their fixed size and position can not be guaranteed.

3.2 Software Analysis

Multimodality has increased its prevalence in the scientific research community, leading to a need to create new, more sophisticated, and specific software tools for the analysis and manipulation of medical data sets. In this project, the RCP-PET images are transformed and then fused with the original MRI images.

In order to develop an algorithm for automating the co-registration of images obtained through a pre-clinical RPC-PET system and its image fusion with an animal magnetic resonance system efficiently, a few platforms were tested for data processing such as 3D Slicer, IDL, AMIDE, and Matlab. In Table 3.2 we present a comparison between tested platforms for data processing. Parameters like

extensibility, portability between platforms, reading and writing tools, and price was also explored.

In the next sections, we present the analysis performed in the programming platforms tested.

Table 3.2: Comparison between tested platforms for data processing. IDL offers a solution that supports medical standards, and also meets medical image analysis and software development requiriments with DICOM specific modules that integrate seamlessly with clinical workflow.

Software name	Remarks
Sicler 3D	Noncommercial, multimodal, image viewing and fusion
MATLAB	Commercial, multimodal, image viewing
IDL	Commercial, image viewing and fusion, design for medical applications, support for interface and display conventions common in clinical environment
AMIDE	Noncommercial, image viewing and fusion

3.2.1 Interactive Data Language (IDL)

Interactive Data Language (IDL)[3] is a dynamic programming language intensely used in interactive processing of large amounts of data, including astronomic and medical imaging. The digital image processing and the security on data transfer, stand out as its major advantages [55].

The extensive library of prebuilt analysis and visualization routines and the built-in support for different data sources and file formats make IDL a flexible and easily adjustable platform. It also allows data transfer from remote servers, as well as writing files at a remote disk using common communication protocols. IDL efficiently integrates with medical equipment consoles and with different acquisition software. The development environment and pre-built protocols make IDL an intuitive, modern code interface that can be easily used.

The described characteristics show that this tool may play an integral role in medical research advancements. It includes solutions that not only support

[3]https://www.harrisgeospatial.com/Software-Technology/IDL

medical image visualization standards, but also meet medical image analysis and software development needs. The add-on module available to handle DICOM files presents a great asset to medical image visualization and analysis.

IDL is a commercial platform, suitable for different operative systems, including *Microsoft Windows*, *Mac OS X* and *Linux*.

Pre-existing co-registration algorithms may be useful to the development of the GUI we intent to design. This platform has played an integral part in medical imaging technology, being used by different members of the medical community with clinical or research goals.

3.2.2 3D Slicer

3D Slicer[4] emerged by the fusion of several independent projects focused on image visualization, surgical navigation, and GUI. It presents an enabling platform for quantitative image computing research. Since its creation, Slicer has been in continuous development. In the last decade, it became an integrated platform used as an orientation, visualization, and analysis tool in a large number of clinical and pre-clinical research applications. Nowadays it can be considered as an industrial software package [56].

It is a free open source software application, that allows the development and distribution of new tools based on pre-existent source code, available to multiple operative systems. It may be distributed freely for academic and commercial use. However, its license makes no claims about the clinical applicability of the software, therefore, the appropriate safety and ethic guidelines are the responsibility of the user.

Slicer provides a set of core functionalities and tools which favor the development and validation of medical image computing methods, thus allowing to understand if a certain function can be executed. Slicer enables the visualization of the different aspects of the images applying basic processing steps and allowing the exploration of the image datasets in two, three or four dimensions.

[4]https://www.slicer.org

Both generic and specialized tools provided by Slicer offer the ability of merging functional and anatomical data. Data processing and multimodal analysis tools are also available. However, it is often required for processing and analysis methods to be initialized manually in order to maintain their robustness.

Slicer is the platform used at ICNAS for the co-registration of the small animal MRI with pre-clinical RPC-PET images, as represented in figure 3.3. Its major disadvantage is the manual process of fusion for each pair of images which increases the processing time and leads to a considerable need of human resources.

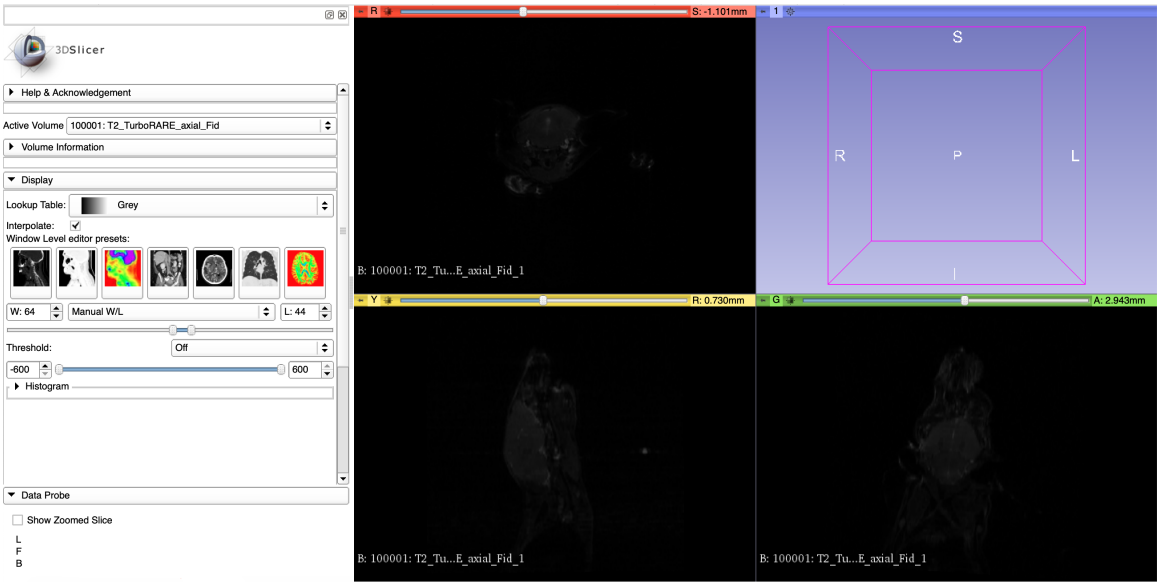

Figure 3.3: 3D Slicer window for DICOM images. Transaxial, sagital and coronal views of an MR image and the display functionalities of the software. The data displayed was obtained at ICNAS with mice.

3.2.3 Matlab

Matlab[5] is a programming platform for the development of data analysis and visualization algorithms. It has a wide range of applications including signal and image processing, control and test projects, financial analysis, among others. A specific tool for image processing - Matlab Image Processing Toolbox - provides a large number of graphic tools for image treatment, as well as, for algorithm development for new applications. Matlab also supports for DICOM data [16]. In

[5]https://www.mathworks.com

figure 3.4 an example of the visualization window DICOM files is presented. Data is presented sequentially which difficult the volume interpretation.

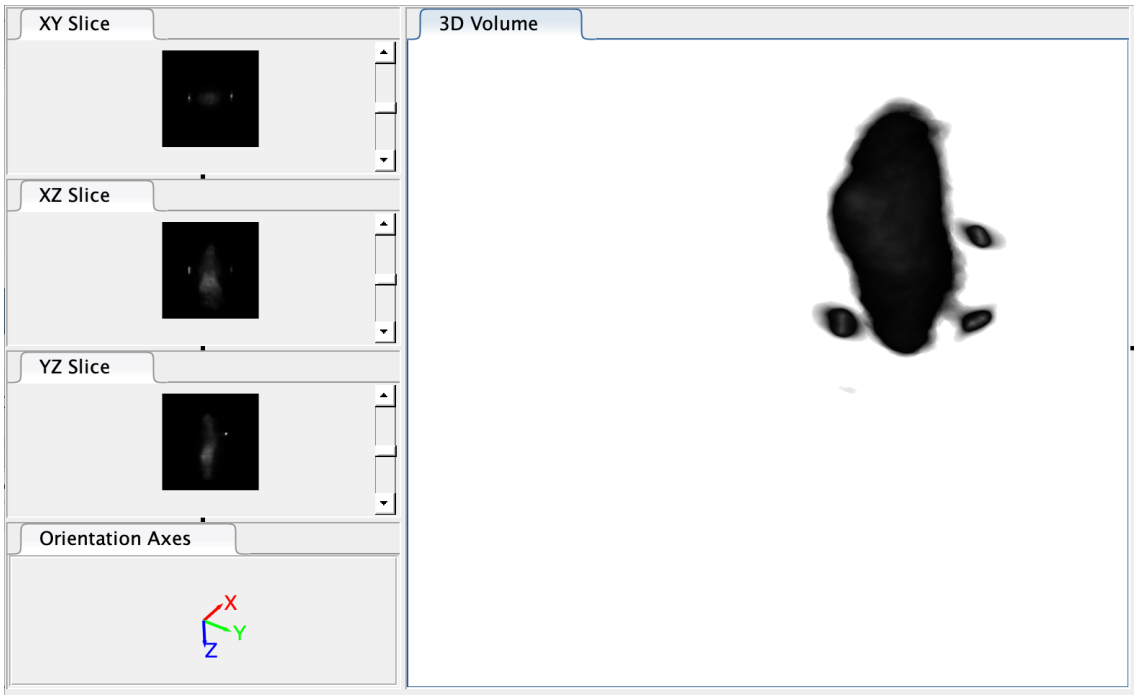

Figure 3.4: Matlab window for 3D visualization of volumes. Transaxial, sagital and coronal views on the left and 3D reconstruction on the right. The MR images displayed was obtained at ICNAS with mice.

Many researchers use Matlab for scientific computation tasks, mostly for initial prototyping and specific GUI creation. Matlab is a generic prototyping tool that is not designed for medical applications and has no support for interface and display conventions common in clinical environments. Being so, to minimizing dependencies and simplifying its clinical integration, medical tools developed need to be translated to more generic programming languages [56].

3.2.4 Amide's Medical Image Data Examiner (AMIDE)

Amide[6] - Amide's Medical Image Data Examiner - is an advanced tool for displaying data and analyzing multimodality volumetric medical images. Amide's software package is a user-friendly, open-source tool, with the ability to simultaneously show multiple data sets and the Regions of Interest (ROI) selection.

[6]http://amide.sourceforge.net

Additionally, as the access to source code is free, users can not only change it, but also expand it for specific assignments. The package includes support for handling data in various formats, one of them being volumes in DICOM format. It has been designed to avoid organization constrains, so data sets and ROIs are logically organized within a tree structure so that many of these items can be simultaneously displayed, modified and analyzed.

The simplified graphic interface and the simple tools allow for an intuitive volume manipulation, as well as the possibility of manual co-registration based on fiducial markers. The image fusion has to be done manually by identifying the markers in the different volume layers.

Figure 3.5 shows a display window of the AMIDE package. From left to right, the orthogonal view of a Computed Tomography (CT), the fused image and a PET image can be observed clearly. Color scales are adapted to fit the images, allowing to see clearly the fiducial markers and other anatomical structures of interest [57].

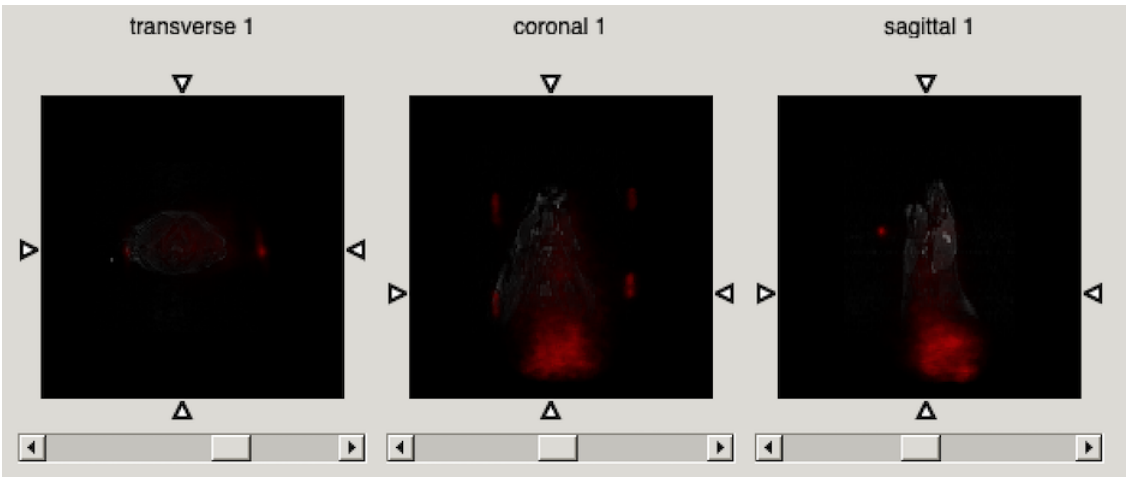

Figure 3.5: Amide coregistration window. Transaxial, sagital and coronal views of merged RCP-PET and MRI volume merged manually. The images displayed were obtained at ICNAS with mice.

However, even though it is a versatile software, the set of features particularly available for image manipulation is limited. The package has been designed emphasising the molecular imaging research, having only a few tools for the volumes we intent to study in this project.

3.2.5 Discussion and Conclusion

The primary aim of the current project is to automate as much as possible the co-registration process of images obtained through a preclinical RCP-PET system and its fusion with an animal magnetic resonance system. With that purpose we intend to create a GUI that can be easily implemented at ICNAS where the data acquisition and pre-processing is made.

Image processing tools currently in use were analyzed taking into account the breadth of functionality, extensibility, cross-platform portability, and non-restrictive software license, as well as the applicability future in the clinical environment. The analysis seeks to select the most adequate platform available for the creation of the co-registration GUI.

For the Matlab evaluation, we can conclude that, despite its wide range of data processing tools, being a prototyping tool limits its integration in the hospital environment and in future clinical applications of the project. In its turn, AMIDE and 3D Slicer platforms allow only manual image fusion and present restrictions on the image processing tools which make them less suitable for creating the desired automatic interface.

Regarding the desired features and functionality, it can be concluded that IDL software package is the most appropriate tool. Although it is a commercial tool, it was considered that the cost is largely justified by the complex medical imaging tools provided by the program, and for its easy integration with pre-existent medical equipment and software. Data security, digital image data processing time and efficiency in applications that require real time analysis were also highlighted.

3.3 Registration Algorithm Design

In this section, the development process of the co-registration algorithm using Interactive Data Language is introduced. The main steps implemented are then described in detail.

For the registration algorithm to be semi-automatic, a landmark measurement method should be used. According to the data features and the literature reviewed ([47, 42, 22, 44]) the most intuitive approach is to identify the landmarks and use their location as a starting point of the co-registration algorithm. A block diagram of the algorithm implemented is shown in figure 3.6.

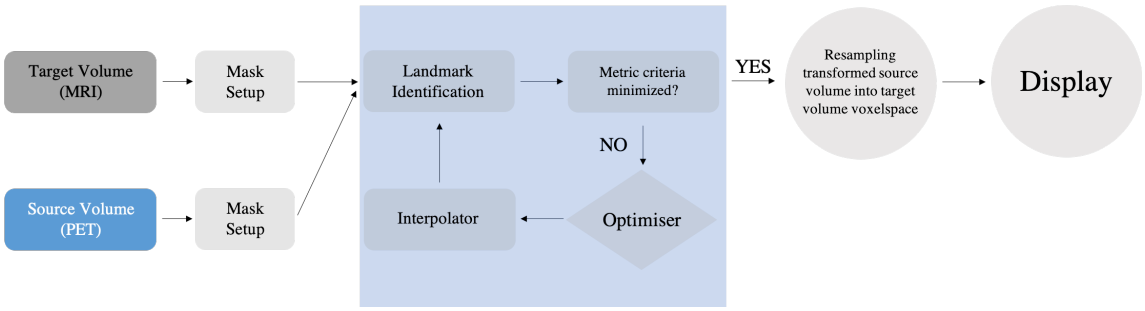

Figure 3.6: Schematic representation of the semi-automatic registration algorithm. MRI and PET volumes are loaded into the program and the body of the mice is selected by the user. Landmarks are then localized and the position of its centroids determined. The functions that co-relate these position are calculated in an iterative process in order to find the scale and offset parameters that minimize the metric's criteria. Once found the final transformation, the source image is resampled into the static physical space of the source image. The pair of the images now co-registered are displayed in a widget.

The fiducial markers are placed in such a distance from the body of the rat that ensures that they can be easily distinguished by its location and geometry. They have a higher activity than the activity observed in the mice which guarantees that the landmarks are highlighted in the images. In order to ensure that the registration algorithm accurately identifies the location of the five markers without taking into account parts of the body of the animal, its body must be selected by the user.

The coordinates of the selected area are then used to design a mask that hides the body. Next, the algorithm seeks the markers considering only the outer side of the images where they are placed. Once they were found on both volumes, the position of their centroids are computed (Figure 3.6) and the functions that relate their positions are optimized in order to achieve the parameters that ensure the registration.

Geometry or feature-based metrics are also implemented to compute the alignment degree between the pair of the images [44]. Volumes are then interpolated with

respect to the parameters found on the optimization calculus and the final co-registered volumes are displayed.

3.3.1 Load data and mask setup

PET and MRI data from the same subject are chosen by the user sequentially, they are loaded into the GUI that allows the user to select the body of the mice by sketching a rectangle surrounding it. According to its body structure, this selection is made on an image of the transaxial projection of the maxima and is then propagated along the z axis. This procedure is made for both volumes as illustrated in Figure 3.7. The code implemented was developed in the Integrated Development Environment (IDE) of the IDL and can be found on Appendix A, figure A.1.

The coordinates of the defined block are used to implement a mask on the original volume, voxels inside that volume are set to zero and they no longer contribute for later intensity measurements in the landmark identification procedure.

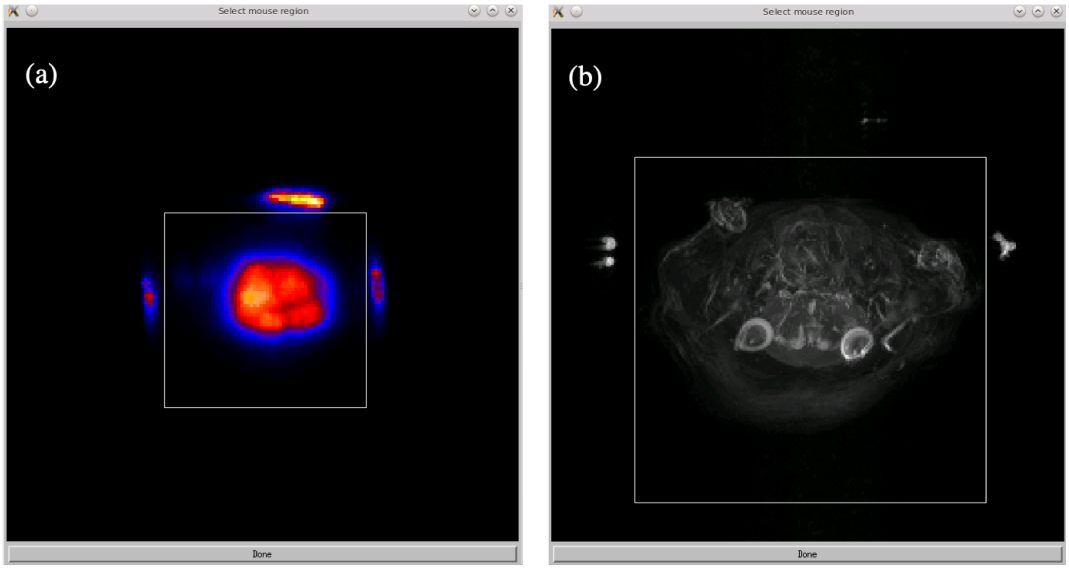

Figure 3.7: GUI used for mask selection. The rectangles are drawn by the user and the program saves their coordinates. Voxels inside the rectangle are set to zero and the rest of the image is maintained unchanged. PET and MRI mask selection, (a) and (b) figures, respectively.

3.3.2 Landmarks identification

Co-registration based on landmarks measurement involves identifying corresponding 3D points in the images to be aligned. After the mask selection and implementation, volumes without the body of the mice are used for landmark identification and segmentation.

Using pre-existent IDL procedures, maximum and minimum intensity values of the volumes are found by inspection, and used as bounds for threshold. Values of the threshold are iteratively increased and the volume is scanned at each iteration (Figure 3.8 illustrates the indexing scheme of IDL). Using the *LABEL REGION* procedure, the connected regions in the volume are automatically identified and a unique integer value is assigned to each one. The volumes are then divided into foreground and background voxels, by thresholding. The iteration stops when only five regions corresponding to the fiducial markers are found, at this step higher and lower threshold values were found and saved.

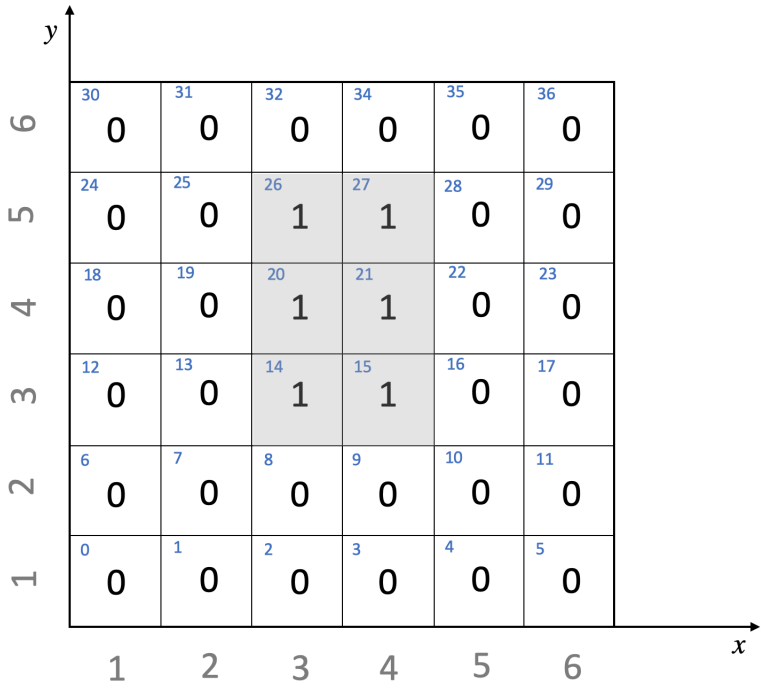

Figure 3.8: Array index scheme (a plane is used for simplicity). Pixels could be identified by their value (black numbers), their index (in blue) or their coordinates (in grey). Index order is followed by the iteratively scanning procedure.

For each one of the regions found, x, y and z coordinates are found, the location

of their centroids are calculated by computing the mean value of its pixels. This segmentation procedure is implemented for both PET and MRI volumes and the code of its main functions can be found on Appendix A, Figure A.2 and A.3.

As a security measure, centroids positions are sequentially analyzed and swapped in case they are out of order in the volumes. Centroid positions in terms of percent of PET and MRI volume, as well as the ratios os centroids positions are computed and printed to analyze the accuracy of the method.

3.3.3 Optimization procedure

Once the positions of the centroids of the fiducial marks of a set of volumes are determined, we need to pursuit the parameters that allows the co-registration, i. e. the conversion of PET volume onto the MRI space. Besides, a registration metric must be implemented in order to quantify the alignment degree achieved in the co-registration process of a pair of imaging studies.

Let A and A' be a pair of fiducial markers, their positions are described in the three dimensional space as x_A, y_A and z_A and $x_{A'}$, $y_{A'}$ and $z_{A'}$, where A index stands out for markers on MRI volume and A' for PET volume, as represented in Figure 3.9. For the co-registration process the parameters used to transform source volume (PET) onto the target (MRI) physical space must be established.

Following [44], equation 3.1, we have that the new PET location (A'') is related to their original location through offset and scale factors, Δx, Δy, and Δz, and f_x. f_y, and f_z, respectively. These six parameters must relate original PET and MRI centroids location information.

$$\begin{cases} x_{A''} = x_{A'} \cdot f_x + \Delta x \\ y_{A''} = y_{A'} \cdot f_y + \Delta y \\ z_{A''} = z_{A'} \cdot f_z + \Delta z \end{cases} \tag{3.1}$$

For point-matching, the coordinates of the correspondent pairs of landmarks must be used to define the registration metric. The registration or similarity metric, R is

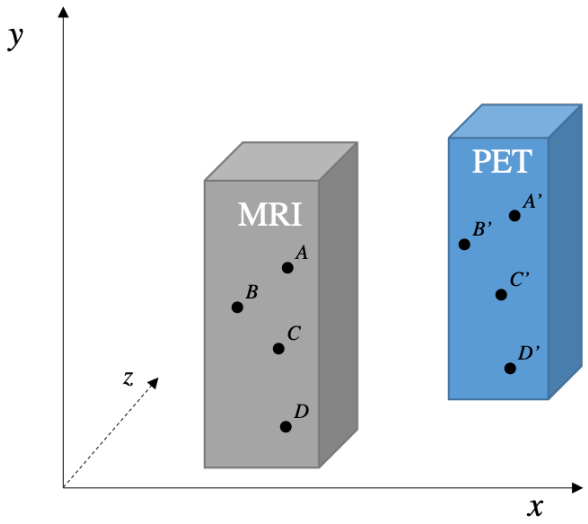

Figure 3.9: Data volume representation (blocks are used for simplicity). Points A, B, C and D represents the centroids of the fiducial markers and have coordinates x_A, y_A and z_A, $x_{A'}$, $y_{A'}$ and $z_{A'}$, and so on.

defined as the sum of the root squared distances between analogous points according to equation 3.2 where i are the centroid index.

$$R = \sum \sqrt{(x_i - x_{i''})^2 + (y_i - y_{i''})^2 + (z_i - z_{i''})^2} \tag{3.2}$$

Using an optimization function designed for this project (Appendix A, Figure A.4 e A.6), the parameters of equation 3.1 were iteratively manipulated until the metric applied was minimized and the set of parameters of transformations that provide the best alignment possible between the pair of volumes is achieved [44].

3.3.4 Interpolation and Transformation

Since PET and MRI volumes have different sizes and are acquired in slightly different positions, an interpolation step is necessary for an accurate merge process. In figure 3.10 the problem is highlighted, blocks are used as representations of the MRI and PET data volumes. Besides volume size and position, also voxel size is different in images acquired from different imaging modalities techniques and we need to ensure that images are in the same physical space [16].

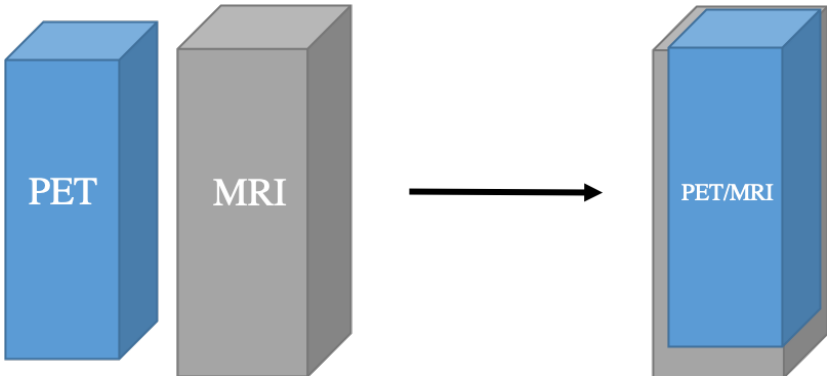

Figure 3.10: Data volume representation, PET volume in blue and MRI volume in grey, the different position and dimensions of the blocks emphasize the differences in volumes under study. As the volumes have different dimensions, fusion without volume interpolation leads to accuracy errors, as shown by the representation of the superimposition of the two blocks.

The interpolation process resides in resampling one image on the grid corresponding to the voxels in the other. The location of each voxel in the transformed image is transformed back to the appropriate location in the original image and the nearest voxel value is copied into the transformed voxel. The parameters that allow the transformation are calculated by the optimization procedure described above. Figure 3.11 illustrates the differences between the positions of the voxels and their positions in a generic pair of images.

In this particular case, we want to transform MRI data, which is a high resolution modality, with voxel size of $0.1758 \times 0.1758 \times 0.500$ mm^3 onto the voxel grid of PET with a voxel size of $0.500 \times 0.500 \times 0.500$ mm^3. As the MR images are shrunk the interpolation will result in a certain loss of information. On the other hand, if we choose to transform PET images onto MRI grid memory required to store PET image will substantially increase - as demonstrated in figure 3.12.

As PET volume are the source, they are the one which are transformed to the MRI grid. The voxels size and coordinates of the minimum position of each volume are used to initialize the interpolation process, then each line of voxels beginning in the location of the minimum position is scanned and the values of both grids are calculated. Coordinates of MRI grid are converted for PET index coordinates and volume interpolation is made using the pre-existent function of IDL *interpolate()*. It must be noticed that the interpolation process also takes into

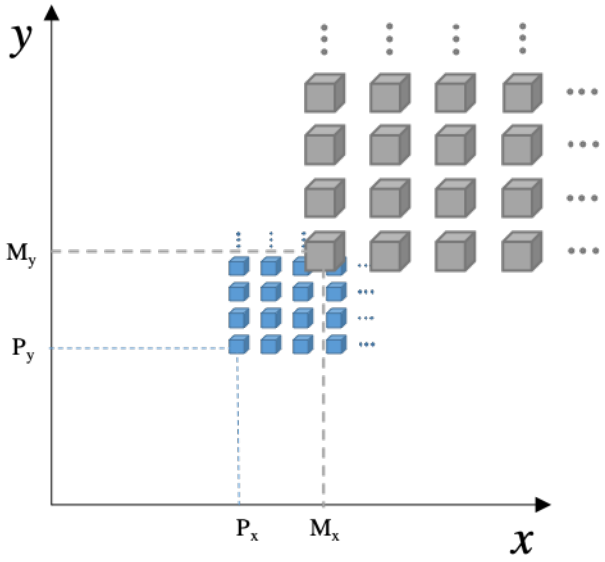

Figure 3.11: Schematic representation of the voxels of two different images under study. Voxels of PET images are represented in blue and have dimensions of $0.500 \times 0.500 \times 0.500$ mm^3, voxels of MR images are in grey and have dimensions of $0.1758 \times 0.1758 \times 0.1758$ mm^3. P_1 and P_2, and M_1 and M_2 stands out for the coordinates of the minimum position of each image.

account the parameters obtained in the optimization process explained in the previous section, so the transformation is applied during the interpolation process. As a result, we obtained the PET data, resampled and co-registered in which fiducial markers are aligned with the MRI data.

The part of the registration algorithm implemented to interpolation and transformation of the PET image can be found in figure A.6 of Appendix A.

3.3.5 Visualization

Co-registered volumes are displayed in a GUI, coronal, axial and transaxial profiles are shown and a slider allows the user to scroll through slices in each one. Changes on the color blending of the volumes and settling different color scales are also possible, was well as zoom in and out.

The cursor position over the surface, gives the user a set of information, such as, the coordinates of the point and the value of each volume. Minimum and maximum values of intensity of both images are also displayed.

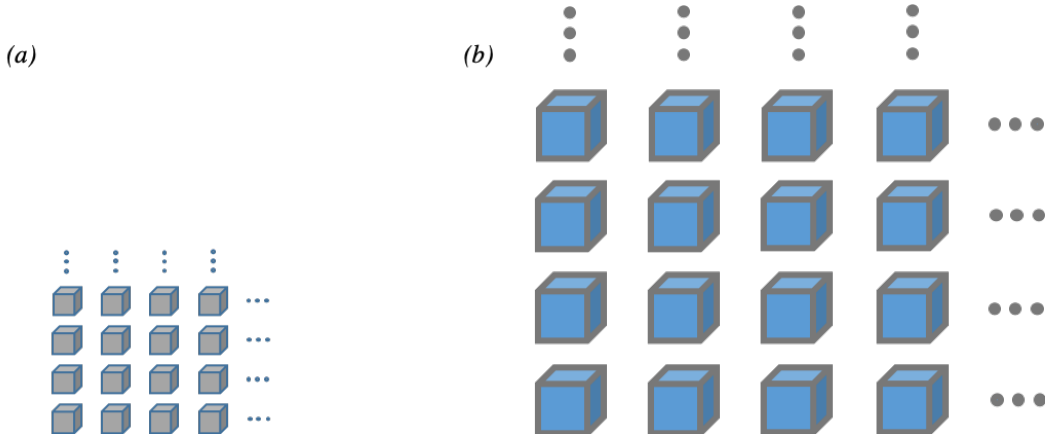

Figure 3.12: Data volume representation after interpolation. Figure (a) shows MR images onto the grid of PET, while figure (b) represents PET images onto MRI grid.

The widget also allows the user to load a couple of images and start a new co-registration process.

3.4 Validation

Validation of an algorithm or procedure refers to the evaluation of the overall techniques in order to ensure the accuracy of image registration and performance criteria on a consistent basis for the intended use.

Validation processes may lead to both qualitative and quantitative results. While the implementation of qualitative methods depend on the tools provided in the image registration software, quantitative results are strongly related with the expertise of the user to interact with the registration results. In both, the analysis of the results requires medical expertise.

Qualitative approach is related with visual inspection, and interpretation of the similarity measure criterion directly. Contour and structures of the anatomical and fiducial markers in the overlaid volumes must be interpreted, an accurate co-registration results in a perfect matching of the surfaces. Multiple overlay displays allowing application of different color scales and blending fractions may also support the visual inspection procedure [44].

One quantitative measure of accuracy registration is given by the distance between a pair of corresponding fiducial markers after registration and transformation. This value is given by the minimum value of the metric function (Equation 3.2) divided by the number of fiducial points used and is known as Target Registration Error (TRE). Hence, more accurate registration is achieved by closer location of the centroids in both volumes. This is the result of a smaller distance between them and, consequently, lesser TRE is accomplished.

In this MRI-PET co-registration application, both quantitative TRE and qualitative visual inspection methods are used to asses the reliability of the algorithm and visualization tool.

4

Results

This chapter presents the performance results for the co-registration method of RPC-PET and MRI volumes system developed in this work. In the first section, considerations about the imaging studies analyzed are introduced. Afterwards, the performance of the co-registration algorithm is presented and the analyzes of four data sets are used as illustrative. This study is divided into co-registration process, including all steps that lead to the determination of the transformation, and co-reregistered volumes, where the fused volumes are presented. The visualization subsection contains an assessment of the GUI.

4.1 Implementation

The co-registration algorithm designed was tested using data acquired from mice between September 2018 and August 2019 using the acquisition equipment and setup described earlier in Section 3.1. To ensure that the subject configuration remained unchanged as much as possible between imaging sessions, the same bed and immobilization device were used on both acquisition devices and the time interval between RCP-PET and MR imaging was minimized in order to reduced physiological changes fo the subject.

For PET data acquisition, mice were intravenously injected with radionuclides labeled with several nucleus and the data was saved on $160 \times 160 \times 160$ matrices with a 0.500 mm pixel size, and slices and 0.500 slice thickness. The MRI scans were acquired on a 4.0 T field using T2-weighted sequences with variable echo and

repetition times, and the data was recorded typically in 256 × 256 matrices with variable number of slices, 0.1758 pixel size, and 0.500 mm slice thickness. All reconstructed data after pre-processing steps were stored in DICOM format, which is the input format of the co-registration algorithm.

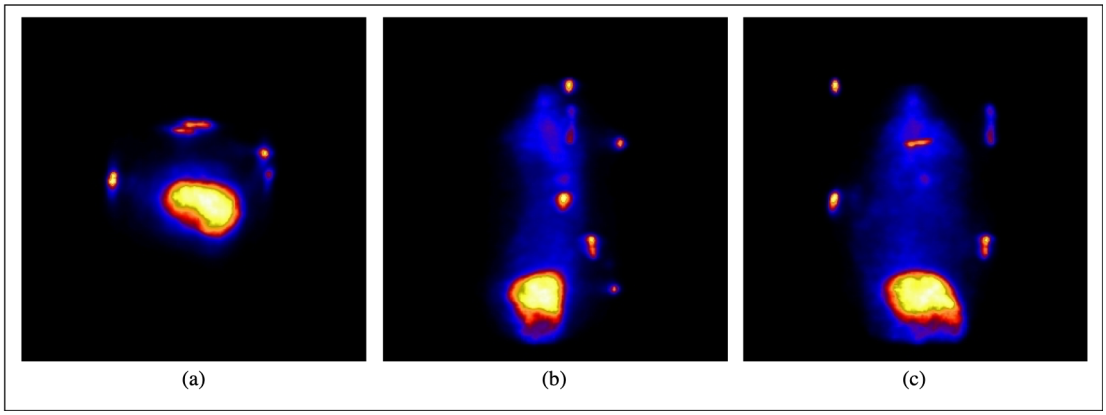

Figure 4.1: RPC-PET maximum intensity projections, sagital (a), coronal (b) and transaxial (c) views. Acquisition was made after injection of a tracer labeled with ^{64}Cu.

Observation of the maximum projections of the PET data shows great variability depending on the uptake time of the radiotracer used. Also, MRI volumes show considerable differences depending on the imaged region of the animal and acquisition parameters used.

For 19 of the studies under analysis, in which radiotracers containing ^{18}F and ^{11}C were injected for RPC-PET acquisition, data was successfully loaded, co-registered and displayed. In the case of the cardiac studies, using NH_3 $-^{11}$ N available, the co-registration was not accomplished. Also for RPC-PET studies that used ^{64}Cu nucleus, the co-registration algorithm failed. As illustrated in figure 4.1, these studies resulted in higher activity in some tissues of the body of the mice than on the fiducial markers. The signal of the regions of the volume corresponding to the landmarks is lower than expected, and as a consequence the landmarks are not found and the method fails. To prove repeatability, each data set was co-registered three times.

4.1.1 Co-registration process

The co-registration process started with the manual selection of the mice for each volume and its application on the original volumes. After the application of the mask, the threshold method found the intensity values of both volumes in which five regions were distinguished and the positions of the landmarks were recorded. For landmarks identification, the algorithm works with the mean value of the maximum and minimum value of the threshold.

For A and B studies, mice were injected with a radiotracer labeled with ^{11}C (Study A and B). Figures 4.2 (a) and (b), and 4.3 present the maximum intensity projections for MRI and RPC-PET data for both modalities.

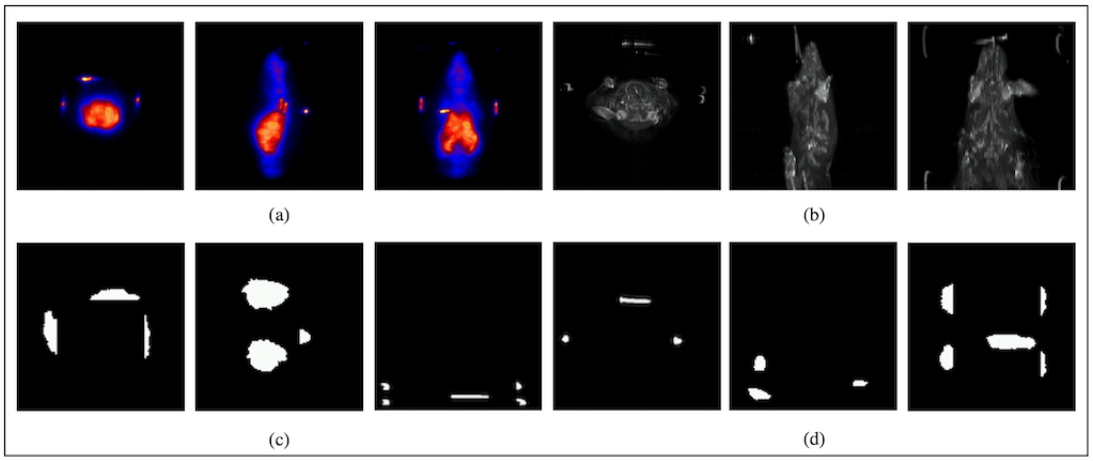

Figure 4.2: Small animal ^{11}C study (Study A). Images (a) and (b) show maximum intensity projections of complete RPC-PET and MRI volumes, respectively. On images (c) and (d) projections of volumes after the application of the masks with underground pixels and pixels inside of the mask set to 0 and foreground pixels set to 1.

In study A, the computational analysis of the intensity profile results on a mean threshold of 2014 (arbitrary units) for MRI volume and 622 (arbitrary units) for PET data. The regions identified over the different volume projections are shown in Fig 4.2 (b) and (c). The mean threshold values calculated for volumes of study B were 1948 (arbitrary units) for MRI and 489 (arbitrary units) for RPC-PET data. However, it is important to notice that the fiducial marker placed under the bed, is much clearer in study A than in study B. The different sizes of the landmark region identified after the application of the mask were a result of the appearance of

the fiducial markers under each acquisition technique, and from the intensity of the markers during it. It is to be expected that the fiducial markers could be treated as point sources by finding the location their centroids, however, the cylindrical shape of the markers causes a spread out of activity during the acquisition.

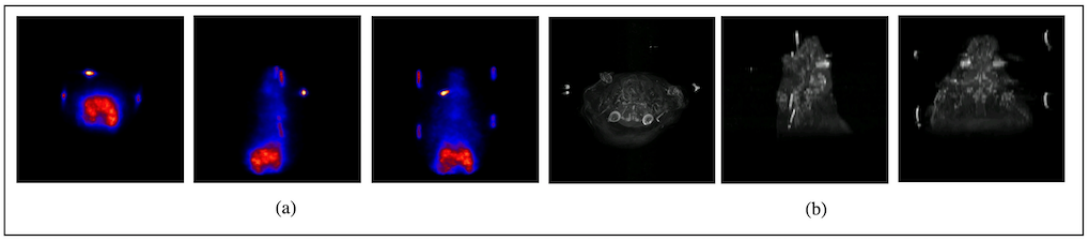

Figure 4.3: Small animal ^{11}C study (Study B). Images (a) and (b) shows maximum intensity projections of complete RPC-PET and MRI volumes, respectively.. For the RPC-PET study, mice was injected with a substance containing ^{11}C

Figure 4.3 presents the transaxial, coronal and sagital views of a study acquired using nucleus of ^{18}F. Significant uptake of FDG in the bladder and neighboring region of the body of the subject results on a higher intensity in the PET images, as illustrated in figure 4.4 (a) by the yellow coloration. In the MRI projections of the abdominal region (image (b)), the fiducial markers placed along the bed can be identified, having higher intensities than the ventral one. Mask setup and threshold calculation result on small landmark regions due to much higher values of the threshold (images (c) and (d) of the figure).

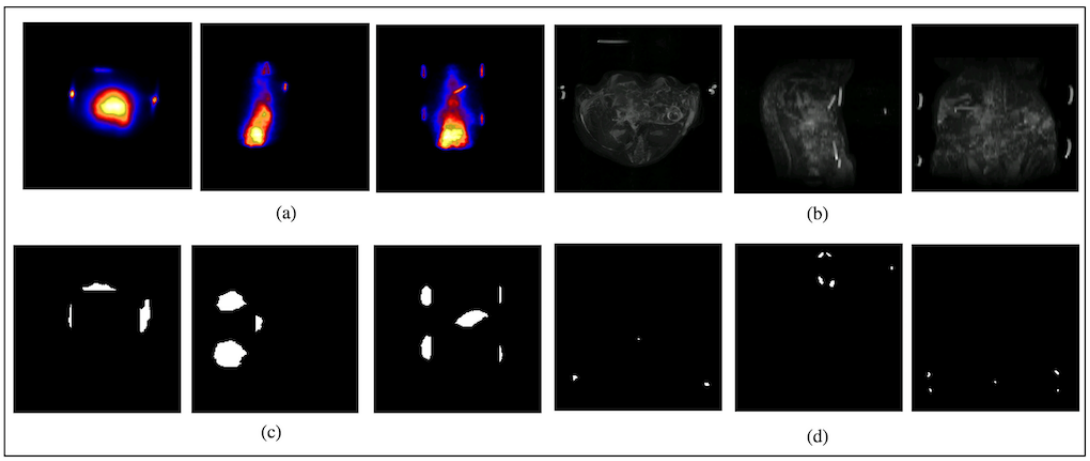

Figure 4.4: Small animal FDG study (Study C). Images (a) and (b) shows the maximum intensity projectons of complete RPC-PET and MRI volumes, respectively.. Images (c) and (d) illustrates the volumes after the application of the frames spotlighting the the landmark regions in both volumes.

For case study D, the acquisition setup was changed. While the RCP-PET scan was performed with a subject labeled with ^{11}C at the end of the uptake time, the MRI volume was acquired without the animal. The same algorithm was applied to this pair of images to obtain the positions of the centroids of the fiducial markers and figure out if, and how, the animal influences the landmark identification. The absence of the subject on the MR acquisition leads to a much lower value of threshold since the landmarks are easily imaged. Projections of the pair of volumes are shown in figure 4.5.

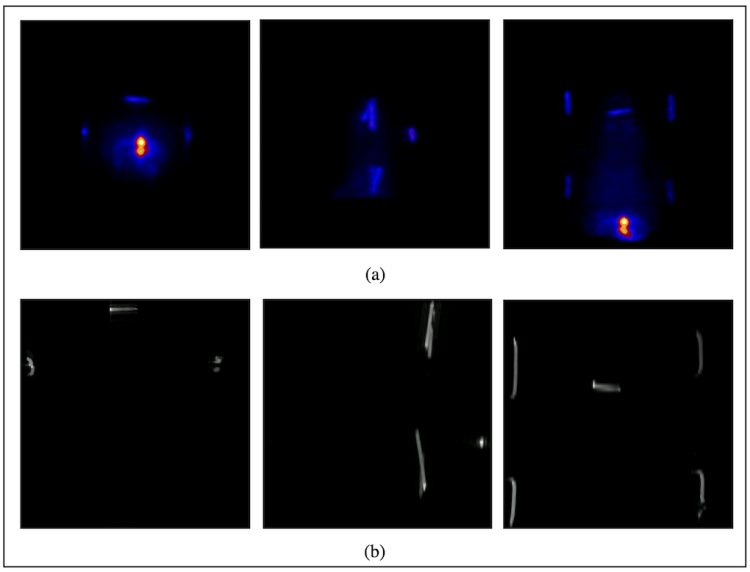

Figure 4.5: Maximum intensity projections for study D. RCP-PET acquisition was made with mice and MR scan was performed without the animal (Study D).

After the application of the frame, the location of the centroids of the fiducial markers were determined and the scale and offset parameters were calculated by the interpolation algorithm, following the steps described in Chapter 3.

Table 4.1 summarizes the position of each of the five fiducial markers before the interpolation process and the values on RPC-PET after interpolation for each study presented. It is important to remember that only the RPC-PET volume was manipulated since it is the source volume. The calculation for the Target Registration Error was also included, since it allows to evaluate the accuracy of the transformation.

Table 4.1: Locations of the five fiducial markers and Target Registration Error (TRE) for each data set in pixels. MRI remain unchanged since it is the target volume. RPC-PET values presented are obtained after the optimization and interpolation process. Anterior fiducial markers are identified as 1 and 2, the ventral marker is labeled as 3, and 4 and 5 stands out for posteriors.

N		1			2			3			4			5		
		x	y	z	x	y	z	x	y	z	x	y	z	x	y	z
A	MRI	228.265	135.556	13.118	23.489	139.707	12.371	147.189	214.867	21.218	223.155	139.518	36.545	22.931	138.543	35.999
	RPC-PET	224.383	134.574	11.497	21.244	140.911	13.902	156.794	213.814	19.933	224.598	133.632	35.783	23.794	140.330	36.231
	TRE	5.0294	pixel	0.8842	mm											
B	MRI	231.356	147.663	5.725	26.595	147.604	3.386	153.848	229.609	26.574	224.951	168.842	36.492	21.952	151.853	35.031
	RPC-PET	228.251	146.630	5.477	21.384	150.452	4.217	161.382	229.637	25.117	228.919	155.131	34.720	23.649	154.261	35.788
	TRE	6.8755	pixel	1.2087	mm											
C	MRI	233.778	163.024	12.692	29.105	154.272	12.761	133.231	224.982	26.033	232.312	166.154	41.246	26.482	153.836	37.762
	RPC-PET	231.379	166.242	9.305	24.140	158.250	9.927	152.284	226.286	21.806	231.938	156.975	41.517	26.482	153.836	37.762
	TRE	8.1936	pixel	1.4404	mm											
D	MRI	230.974	124.345	28.472	24.239	121.179	21.664	115.467	206.252	40.757	226.504	134.939	70.572	24.704	130.765	68.769
	RPC-PET	227.448	128.737	25.443	24.453	120.082	22.606	120.519	205.280	39.071	226.739	137.068	70.515	24.209	130.187	68.906
	TRE	7.2383	pixel	1.2724	mm											

4.1.2 Co-registered volumes

After the computation of the co-registration algorithm, RCP-PET data was resampled on MRI physical space and volumes were merged. Considering all the data sets successfully registered, the mean value for Target Error Registration (Error) was 1.906 mm.

In figure 4.6 three slices of the transaxial projection are shown, where the five fiducial markers are highlighted. The two anterior markers are illustrated in figure 4.6-(a), the fiducials placed under the body of the mouse can be seen in figure 4.6-(b) and, finally, in figure 4.6-(c) the two posterior ones appear sideway of the mouse body. The application of the similarity measure results in a TRE of 5.029 pixels, which corresponds to 0.884 mm.

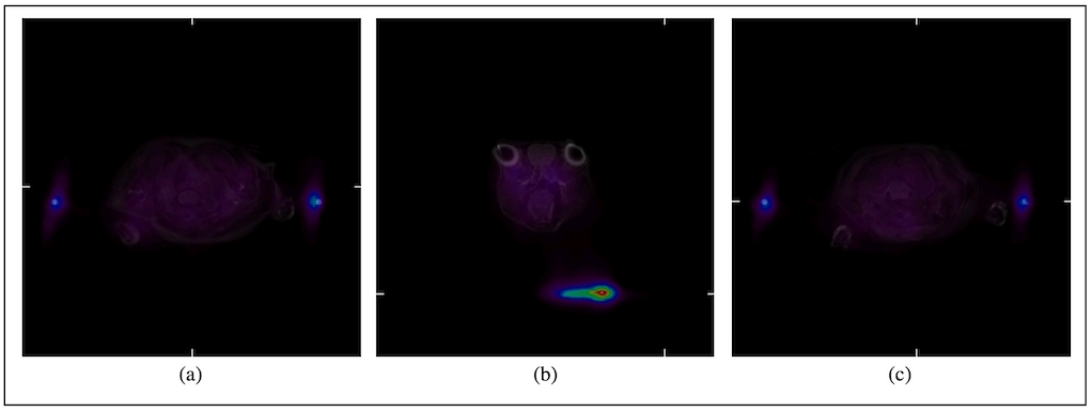

Figure 4.6: Slices of the transaxial projection of the co-registered volume of study A.

Images of case study B were acquired under the same acquisition conditions of images of study A, resulting in their co-registration with a TRE of 1.2087 mm. A transaxial slice of the co-registered volume B is shown in figure 4.10, where one of the fiducial markers could be noticed on the left. Anatomical structures and regions with higher activity are also distinguishable in image (b).

For the case study C, the RPC-PET acquisition was made using FDG instead of $^{11}\mathrm{C} - PK$. The co-registration was achieved with a TRE of 1.440 mm. As demonstrated in figure 4.7 the fiducial marker below the mice seems to appear larger or shifted on MRI volume. The high intensity on the body of the mouse

does not influence the identification of the markers and the registration process.

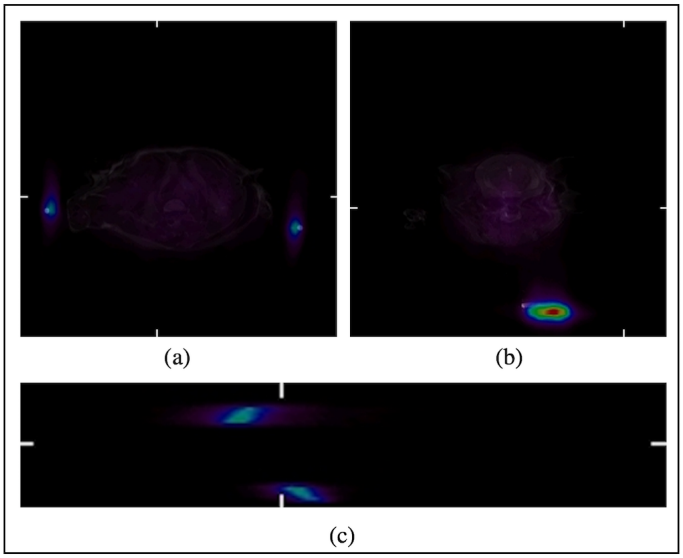

Figure 4.7: Different slices of the merged volume of case study C. While figures (a) and (b) show transaxial view, figure (c) shows the coronal view. All the images focus on the fusion of the fiducial markers.

Regarding the data set D, in which MR imaging was performed without the animal, the co-registration process was accomplished. As a result of the different conditions of acquisition between the two datasets, the fusion of the fiducial markers is emphasized on the final volume (Figure 4.8). On transaxial views, the two grey regions below the lateral markers are image artifacts caused by the bed. For this data set, TRE was about 1.2 mm. It is important to notice that in this acquisition, one of the anterior fiducial markers has a lower intensity having almost no expression on the images presented.

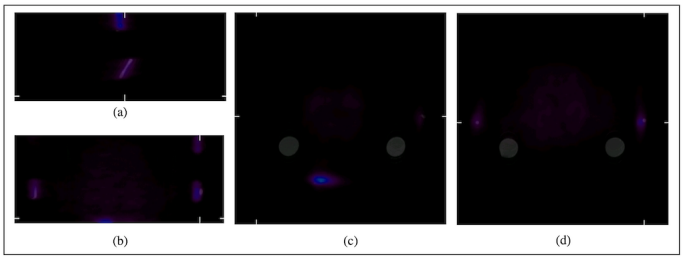

Figure 4.8: Slices of merged volumes of case study D with the five fiducial markers. Sagital projection highlight the co-registration of one anterior marker (a) and coronal projection shows the fusion of three lateral landmarks (b). Transaxial projections show the marker placed below the mouse and the two posterior markers are located sideways, (c) and (d).

4.1.3 Visualization

After the co-registration process is complete, it is mandatory to have an interface that allows to the user to visualize the results and perform simple manipulation steps to support its analysis. In this work, volumes are displayed with the *PET MRI VISUALIZER*, a widget adapted for this goal (Figure. 4.9).

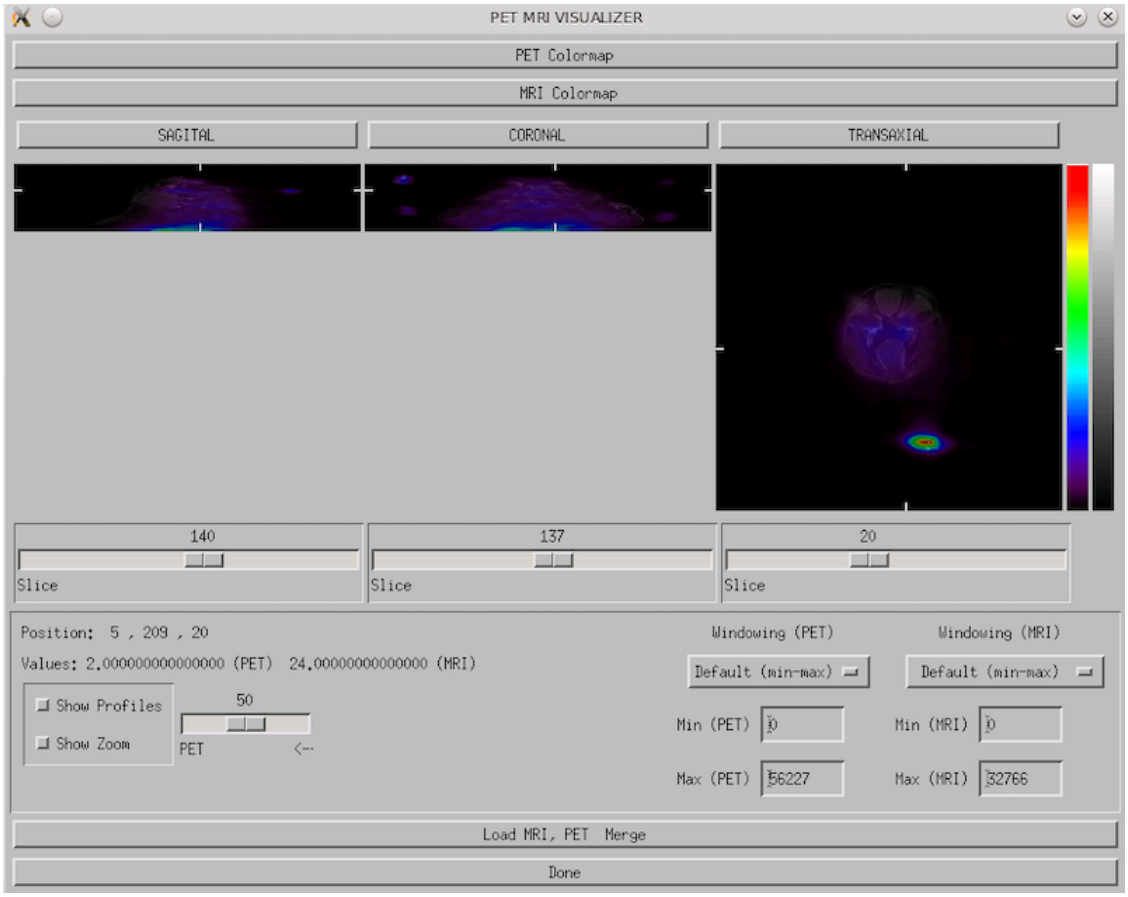

Figure 4.9: Graphical User Interface adapted for visualization and analysis of the co-registration images, allowing small volume manipulation steps and retrieving important information about the volumes under study. Widget also allows loading new studies.

Three display windows allow the user to scan the co-registered volume in the different projections, showing the information about the slice index during all the manipulation. Informations such as maximum and minimum intensity of a particular point or its location could be achieved interactively by putting the mouse above it. Generic information about the volume is also displayed. Blende function (see Figure 4.11), zoom option, and change of the color scale (Figure

4.10) are included to support visual inspection of the co-registered volume.

The color scale bar shown on the GUI, represents the uptake value, with structures with more activity represented in red (as the central point of the fiduciary marker) and areas with low activity represented in blue tones (lower region of the color scale bar). Depending on the data under analysis, changing the color scale might be helpful leading to better contrast among structures or allowing to have more structural detail. The application of different color mapping to the RCP-PET data is illustrated in figure 4.10.

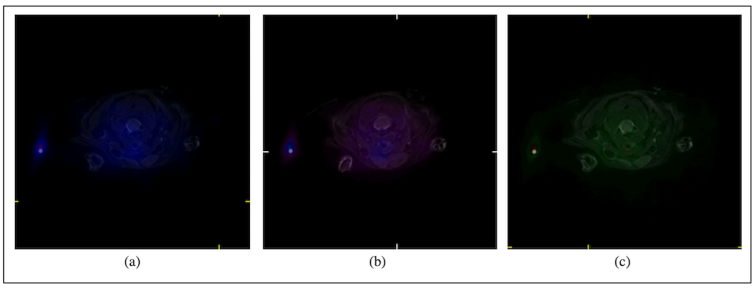

Figure 4.10: Coronal slice of the co-registered volume of data set B with the application of different color scales to the RPC-PET data.

While RPC-PET and MRI provide complementary information, sometimes it is important to evaluate the stand-alone volume instead of the merged. The blend function allows the user to control the fraction of the target and source image presented on the display. In figure 4.11, images of just PET or MRI are presented along the secondary diagonal. The other two images show merged volumes in which different fractions of the PET image is sampled. Low fraction of functional data representations allow the identification of more anatomical details, having in color just the regions with high intensities. Having said this, when more functional data is shown, slight variations in the contrast are identified.

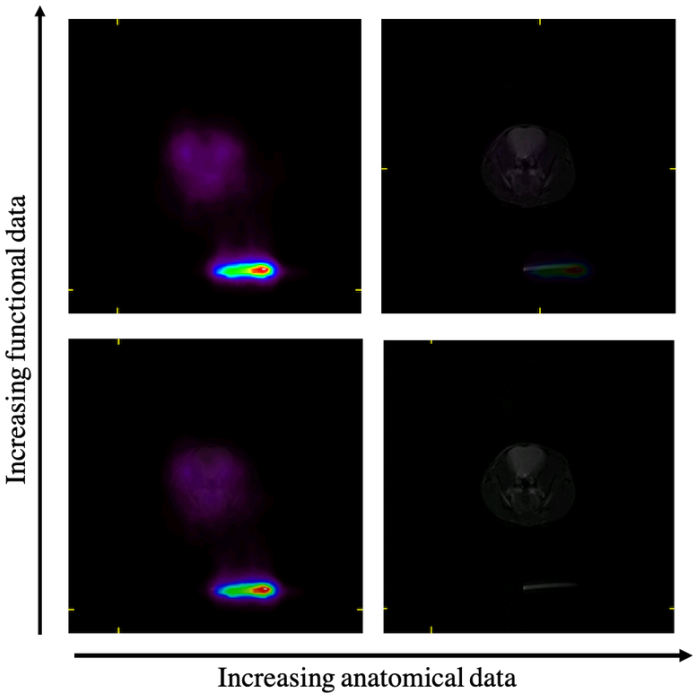

Figure 4.11: Application of the blend function of the GUI to the co-registered volume of case study A.

5

Discussion and Conclusions

The purpose of this project was to design a co-registration algorithm for small animal imaging devices working at ICNAS. With that goal, a registration algorithm was developed in IDL. For visualization and analysis of the merged volumes, a GUI was adapted and, therefore, the objective of co-registering and displaying pre-clinical RPC-PET images with animal MRI was fulfilled.

However, the full automation of the algorithm was not possible due to the high variability of the appearance of the fiducial markers on the images under study. As they are hand-made for each study, their size and composition are not always the same. Since they have no fixed supports, the location where they are placed differ between studies. They are also vulnerable in the process of changing the bed from the RPC-PET to the MRI device between acquisitions. In the first section, the acquisition technologies and main features of the volumes under analysis are presented, with an assessment of the fiducial markers.

To overcome the obstacles imposed by the landmarks design and composition, the developed semi-automated algorithm is supported by the interactive selection of a frame which includes the body of the mouse to be isolated from the fiducial markers. After the removal of the mouse, the algorithm computes the intensity threshold values and finds the location of the centroids of the five fiducial markers in both images. In the next step, the registration parameters are determined by the implementation of the registration metric on the optimization procedure. In the following stage, the transform is applied, and PET volume interpolation is computed. The latter has as output RPC-PET data resampled and transformed in the MRI physical space with the fiducial markers aligned. Co-registered volumes are then

displayed on a GUI.

The performance of the method was evaluated by testing the algorithm in different datasets acquired at ICNAS. The main difference between studies was the radiotracer used for the RPC-PET acquisition. The volumes tested included PET studies using mice labeled with ^{11}C, ^{18}F, $NH_3{-}^{11}$N, and ^{64}Cu. For datasets containing images acquired with the last two, the registration was not accomplished since landmarks are not accurately identified due to their low intensity. In the case of mice labeled with ^{11}C and ^{18}F, the registration was achieved with a TRE mean value of 1.906 mm for the 19 datasets analyzed. It is important to notice that values for studies using ^{18}F were slightly higher. An exact registration of the volumes would arise in the exact same location for every structure, resulting in a TRE of 0. By the definition of TRE presented earlier lower TRE values, indicate minor distances between corresponding points. In practice, there will always be some degree of uncertainty regarding the location of a pair of markers, which could be introduced for the acquired images, for the registration process, and the visualization method used, among others.

The analysis of the volumes acquired in studies A and B (figure 4.2 and 4.3, respectively), shows differences in the activity of the fiducial markers among studies even though they are acquired using the same radiotracer. However, after the application of the mask, the threshold value and the size of the landmark regions present similar values for both RPC-PET and MR images. For the identification of the centroids of the markers before the interpolation, values have a maximum difference of 9 pixels for MRI. After the interpolation, the positions for each marker in both imaging volumes are close and the alignment of these points (figure 4.6) allows the positioning of the entire volume.

In study C, RPC-PET acquisition was based on ^{18}F, resulting in regions with activity on the body of the mouse. The MRI abdomen acquisition also allows imaging all the fiducial markers, even though the structures and tissues represented differ from those from brain acquisitions. Since the signal intensity is higher, there is no well defined border between the markers and the body of the mice and the mask setup may lead to miscalculation of the centroids of the markers. In the case of the MRI imaging, for this type of acquisition, the threshold bound are superior which results

in almost point-like markers. Co-registration of this volume was achieved with a TRE of 1.27 mm. By visual inspection of the transaxial view of the merge volume (Figure 4.7), the position of the markers seems to be misplaced in the x direction. MRI lateral markers seem to be further apart than the same structures in PET volume, which might indicate an error in the calculation of the scale factors or that some sort of distortion was introduced.

The co-registered process was also accomplished for the MRI acquisition performed without the presence of the body of the mice. For the two posterior and the ventral markers, coordinates for the final volumes are very close (Table 4.1). However, for the anterior markers the centroids found are not so similar, which suggests that they are shifted between acquisitions.

Whereas low values of TRE were obtained, subvoxel precision was not achieved with the application of the algorithm, even though the dimensions of the external markers used was much larger than voxel size, and the contrast material used in their construction was visible in both acquisition modalities.

When evaluating the accuracy and error sources present on the process, variations on the positions of the fiducial markers during acquisitions must be noted, as well as differences in their size and composition. As they are built for one time use, their location cannot be used as a reference. The acquisition system could be improved by using commercial markers instead. The registration process is also affected by the acquisition parameter of the registered volumes, mainly by the resolution (size of the voxels) in each volume. RPC-PET studies present lower spatial resolution than the MR volumes, involving significant resizing and resampling operations that affect the values of the reconstructed voxels. The co-registration accuracy is also affected by the soft tissue deformation that occurs due to breathing and cardiac motion, which cannot be totally addressed by imaging protocols. These image artifacts cause inconsistent anatomy and limit the geometric exactness of the image.

The co-registration algorithm can also be a source of error. Since the manual selection of the frame is highly dependent on the user interpretation of the volumes, that step represents a weakness in the developed method. Mistakes in the selection of the mask cause uncertainties in the identification of the features that

drive the registration. The interpolation process could also be incorrectly performed resulting in improper extrapolation of the registration field of view (Figure 4.7).

In conclusion, the overall objectives of the current project were only partially achieved since the system developed is not fully automated. However, semi-automated co-registration of the pre-clinical data under study was accomplished with small TRE value.

The full automation of the system may be considered for future work. Also, improvements on the co-registration algorithm may be made, and the threshold method can be optimized to calculate a tightened range of values and reduce the size of the fiducial regions to point-like structures. Having said this the error associated with the positions of the centroids of the landmarks will drastically decrease, making the transformation more reliable. The reconstruction of the data in an interactive three-dimensional widget may also be accomplished for this type of data representing an intuitive tool for volume analysis by researchers. However, their development and implementation are computationally demanding.

Bibliography

[1] H. Müller, A. G. S. de Herrera, J. Kalpathy-Cramer, D. Demner-Fushman, S. K. Antani, and I. Eggel, "Overview of the imageCLEF 2012 medical image retrieval and classification tasks.," in *CLEF*, pp. 1–16, 2012.

[2] G. B. Saha, *Basics of PET imaging: physics, chemistry, and regulations*. Springer, 2015.

[3] C. Catana, A. Drzezga, W.-D. Heiss, and B. R. Rosen, "PET/MRI for neurological applications," *Journal of Nuclear Medicine*, vol. 53, no. 12, pp. 1916 – 1925, 2012.

[4] F. Alam, S. U. Rahman, A. Khalil, *et al.*, "An investigation towards issues and challenges in medical image registration," *Journal of Postgraduate Medical Institute (Peshawar-Pakistan)*, vol. 31, no. 3, 2017.

[5] P. Martins, A. Blanco, P. Crespo, M. F. F. Marques, R. F. Marques, P. M. Gordo, M. Kajetanowicz, G. Korcyl, L. Lopes, J. Michel, *et al.*, "Achieving 0.4-mm FWHM spatial resolution with an RPC-based small-animal pet prototype," in *Nuclear Science Symposium and Medical Imaging Conference (NSS/MIC), 2013 IEEE*, pp. 1–2, IEEE, 2013.

[6] F. E.-Z. A. El-Gamal, M. Elmogy, and A. Atwan, "Current trends in medical image registration and fusion," *Egyptian Informatics Journal*, vol. 17, no. 1, pp. 99–124, 2016.

[7] F. Alam and S. U. Rahman, "Intrinsic registration techniques for medical images: a state-of-the-art review," *Journal of Postgraduate Medical Institute*

(Peshawar-Pakistan), vol. 30, no. 2, pp. 119 –132, 2016.

[8] J. T. Bushberg and J. M. Boone, *The essential physics of medical imaging*. Lippincott Williams & Wilkins, 2011.

[9] R. Acharya, R. Wasserman, J. Stevens, and C. Hinojosa, "Biomedical imaging modalities: a tutorial," *Computerized Medical Imaging and Graphics*, vol. 19, no. 1, pp. 3–25, 1995.

[10] D. Ganguly, S. Chakraborty, M. Balitanas, and T.-h. Kim, *Medical Imaging: A Review*, vol. 78, pp. 504–516. Communications in Computer and Information Science, 09 2010.

[11] F. Kiessling, B. J. Pichler, and P. Hauff, *Small animal imaging*. Springer, 2016.

[12] B. J. Pichler, H. F. Wehrl, A. Kolb, and M. S. Judenhofer, "Positron emission tomography/magnetic resonance imaging: the next generation of multimodality imaging?," *Semin Nucl Med*, vol. 38, pp. 199–208, May 2008.

[13] H. Wehrl, A. Sauter, M. Judenhofer, and B. Pichler, "Combined PET/MR imaging—technology and applications," *Technology in Cancer Research & Treatment*, vol. 9, no. 1, pp. 5–20, 2010.

[14] T. A. Hope, Z. A. Fayad, K. J. Fowler, D. Holley, A. H. Iagaru, A. McMillan, P. Veit-Haibach, R. J. Witte, G. Zaharchuk, and C. Catana, "State of the art PET/MRI: Applications and limitations-summary of the first ISMRM/SNMMI co-provided workshop on PET/MRI," *Journal of Nuclear Medicine*, pp. jnumed–119, 2019.

[15] M. S. Robertson, X. Liu, W. Plishker, G. F. Zaki, P. K. Vyas, N. M. Safdar, and R. Shekhar, "Software-based PET-MR image coregistration: combined PET-MRI for the rest of us!," *Pediatric Radiology*, vol. 46, no. 11, pp. 1552–1561, 2016.

[16] D. L. Hill, P. G. Batchelor, M. Holden, and D. J. Hawkes, "Medical image registration," *Physics in Medicine & Biology*, vol. 46, no. 3, p. R1, 2001.

[17] D. J. Hawkes, D. L. Hill, L. Hallpike, and D. L. Bailey, "Coregistration of

structural and functional images," in *Positron Emission Tomography*, pp. 161–177, Springer, 2005.

[18] F. Alam and S. U. Rahman, "Medical image registration: Classification, applications and issues," *JPMI*, vol. 32, no. 4, p. 300, 2018.

[19] J. A. Maintz and M. A. Viergever, "A survey of medical image registration," *Medical Image Analysis*, vol. 2, no. 1, pp. 1–36, 1998.

[20] F. Bashiri, A. Baghaie, R. Rostami, Z. Yu, and R. D'Souza, "Multi-modal medical image registration with full or partial data: A manifold learning approach," *Journal of Imaging*, vol. 5, no. 1, p. 5, 2019.

[21] F. Khalifa, G. M. Beache, G. Gimel'farb, J. S. Suri, and A. S. El-Baz, "State-of-the-art medical image registration methodologies: A survey," in *Multi modality state-of-the-art medical image segmentation and registration methodologies*, pp. 235–280, Springer, 2011.

[22] C. R. Maurer, Jr, J. M. Fitzpatrick, M. Y. Wang, R. L. Galloway, Jr, R. J. Maciunas, and G. S. Allen, "Registration of head volume images using implantable fiducial markers," *IEEE Trans Med Imaging*, vol. 16, pp. 447–62, Aug 1997.

[23] J. West, J. M. Fitzpatrick, M. Y. Wang, B. M. Dawant, C. R. Maurer, Jr, R. M. Kessler, R. J. Maciunas, C. Barillot, D. Lemoine, A. Collignon, F. Maes, P. Suetens, D. Vandermeulen, P. A. van den Elsen, S. Napel, T. S. Sumanaweera, B. Harkness, P. F. Hemler, D. L. Hill, D. J. Hawkes, C. Studholme, J. B. Maintz, M. A. Viergever, G. Malandain, and R. P. Woods, "Comparison and evaluation of retrospective intermodality brain image registration techniques," *J Comput Assist Tomogr*, vol. 21, no. 4, pp. 554–66, 1997.

[24] C. A. Pelizzari, G. Chen, D. R. Spelbring, R. R. Weichselbaum, and C.-T. Chen, "Accurate three-dimensional registration of CT, PET, and/or MR images of the brain.," *Journal of Computer Assisted Tomography*, vol. 13, no. 1, pp. 20–26, 1989.

[25] U. Pietrzyk, K. Herholz, G. Fink, A. Jacobs, R. Mielke, I. Slansky, M. Würker, and W.-D. Heiss, "An interactive technique for three-dimensional image registration: validation for PET, SPECT, MRI and CT brain studies," *Journal of Nuclear Medicine*, vol. 35, no. 12, pp. 2011–2018, 1994.

[26] S. Eberl, I. Kanno, R. R. Fulton, A. Ryan, B. F. Hutton, and M. J. Fulham, "Automated interstudy image registration technique for SPECT and PET," *J Nucl Med*, vol. 37, pp. 137–45, Jan 1996.

[27] R. P. Woods, S. R. Cherry, and J. C. Mazziotta, "Rapid automated algorithm for aligning and reslicing PET images," *J Comput Assist Tomogr*, vol. 16, no. 4, pp. 620–33, 1992.

[28] R. P. Woods, J. C. Mazziotta, and S. R. Cherry, "MRI-PET registration with automated algorithm," *J Comput Assist Tomogr*, vol. 17, no. 4, pp. 536–46, 1993.

[29] V. R. Mandava, J. M. Fitzpatrick, C. R. Maurer Jr, R. J. Maciunas, and G. S. Allen, "Registration of multimodal volume head images via attached markers," in *Medical Imaging VI: Image Processing*, vol. 1652, pp. 271–282, International Society for Optics and Photonics, 1992.

[30] M. Y. Wang, J. M. Fitzpatrick, and C. R. Maurer Jr, "Design of fiducials for accurate registration of CT and MR volume images," in *Medical Imaging 1995: Image Processing*, vol. 2434, pp. 96–108, International Society for Optics and Photonics, 1995.

[31] M. Y. Wang, C. R. Maurer, J. M. Fitzpatrick, and R. J. Maciunas, "An automatic technique for finding and localizing externally attached markers in CT and MR volume images of the head," *IEEE Transactions on Biomedical Engineering*, vol. 43, no. 6, pp. 627–637, 1996.

[32] V. Mani and A. Selvaraj, "Survey of medical image registration," *Journal of Biomedical Engineering and Technology*, vol. 1, pp. 8–25, Jan 2013.

[33] L. Lemieux, N. D. Kitchen, S. W. Hughes, and D. G. Thomas, "Voxel-based localization in frame-based and frameless stereotaxy and its accuracy," *Medical*

Physics, vol. 21, no. 8, pp. 1301–1310, 1994.

[34] K. P. Gall, L. J. Verhey, and M. Wagner, "Computer-assisted positioning of radiotherapy patients using implanted radiopaque fiducials," *Medical physics*, vol. 20, no. 4, pp. 1153–1159, 1993.

[35] A. C. Evans, S. Marrett, J. Torrescorzo, S. Ku, and L. Collins, "MRI-PET correlation in three dimensions using a volume-of-interest (VOI) atlas," *Journal of Cerebral Blood Flow & Metabolism*, vol. 11, no. 1_suppl, pp. A69–A78, 1991.

[36] K. Rohr, M. Fornefett, and H. S. Stiehl, "Spline-based elastic image registration: integration of landmark errors and orientation attributes," *Computer Vision and Image Understanding*, vol. 90, no. 2, pp. 153–168, 2003.

[37] S. Periaswamy and H. Farid, "Medical image registration with partial data," *Medical image analysis*, vol. 10, no. 3, pp. 452–464, 2006.

[38] A. C. Evans, S. Marrett, L. Collins, and T. M. Peters, "Anatomical-functional correlative analysis of the human brain using three dimensional imaging systems," in *Medical imaging III: image processing*, vol. 1092, pp. 264–274, International Society for Optics and Photonics, 1989.

[39] M. Nack, "Rectification and registration of digital images and the effect of cloud detection," 1977.

[40] W. Kerwin and C. Yuan, "Active edge maps for medical image registration," in *Medical Imaging 2001: Image Processing*, vol. 4322, pp. 516–526, International Society for Optics and Photonics, 2001.

[41] A. M. Dale, B. Fischl, and M. I. Sereno, "Cortical surface-based analysis: I. segmentation and surface reconstruction," *Neuroimage*, vol. 9, no. 2, pp. 179–194, 1999.

[42] F. Maes, A. Collignon, D. Vandermeulen, G. Marchal, and P. Suetens, "Multimodality image registration by maximization of mutual information," *IEEE Trans Med Imaging*, vol. 16, pp. 187–98, Apr 1997.

[43] C. Wachinger and N. Navab, "Entropy and laplacian images: structural

representations for multi-modal registration," *Med Image Anal*, vol. 16, pp. 1–17, Jan 2012.

[44] K. K. Brock, S. Mutic, T. R. McNutt, H. Li, and M. L. Kessler, "Use of image registration and fusion algorithms and techniques in radiotherapy: Report of the AAPM radiation therapy committee task group no. 132," *Med Phys*, vol. 44, pp. e43–e76, Jul 2017.

[45] J. Ceranka, M. Polfliet, F. Lecouvet, N. Michoux, J. de Mey, and J. Vandemeulebroucke, "Registration strategies for multi-modal whole-body MRI mosaicing," *Magn Reson Med*, vol. 79, pp. 1684–1695, 03 2018.

[46] J. J. Vaquero, M. Desco, J. Pascau, A. Santos, I. Lee, J. Seidel, and M. V. Green, "PET, CT, and MR image registration of the rat brain and skull," *IEEE Transactions on Nuclear Science*, vol. 48, no. 4, pp. 1440–1445, 2001.

[47] N. Hayakawa, K. Uemura, K. Ishiwata, Y. Shimada, N. Ogi, T. Nagaoka, H. Toyama, K. Oda, A. Tanaka, K. Endo, *et al.*, "A PET-MRI registration technique for PET studies of the rat brain," *Nuclear medicine and biology*, vol. 27, no. 2, pp. 121–125, 2000.

[48] B. A. Ardekani, M. Braun, B. F. Hutton, I. Kanno, and H. Iida, "A fully automatic multimodality image registration algorithm.," *Journal of computer assisted tomography*, vol. 19, no. 4, pp. 615–623, 1995.

[49] S. Bricq, H. L. Kidane, J. Zavala-Bojorquez, A. Oudot, J.-M. Vrigneaud, F. Brunotte, P. M. Walker, A. Cochet, and A. Lalande, "Automatic deformable pet/mri registration for preclinical studies based on b-splines and non-linear intensity transformation," *Med Biol Eng Comput*, vol. 56, pp. 1531–1539, Sep 2018.

[50] A. Parsai, M. E. Miquel, H. Jan, A. Kastler, T. Szyszko, and I. Zerizer, "Improving liver lesion characterisation using retrospective fusion of FDG PET/CT and MRI," *Clin Imaging*, vol. 55, pp. 23–28, 2019.

[51] J. G. Mannheim, M. Mamach, S. Reder, A. Traxl, N. Mucha, J. A. Disselhorst, M. Mittelhäuser, C. Kuntner, J. T. Thackeray, S. Ziegler, T. Wanek, J. P.

Bankstahl, and B. J. Pichler, "Reproducibility and comparability of preclinical PET imaging data: A multi-center small animal pet study," *J Nucl Med*, Mar 2019.

[52] N. Beckmann, R. Kneuer, H.-U. Gremlich, H. Karmouty-Quintana, F.-X. Blé, and M. Müller, "In vivo mouse imaging and spectroscopy in drug discovery," *NMR Biomed*, vol. 20, pp. 154–85, May 2007.

[53] M. Couceiro, P. Crespo, A. Blanco, N. Ferreira, L. Mendes, R. F. Marques, and P. Fonte, "Time-of-flight positron emission tomography with resistive plate chamber detectors: An unlikely but promising approach," *Acta Physica Polonica A*, vol. 127, no. 5, pp. 1453–1461, 2015.

[54] P. Martins, A. Blanco, P. Crespo, M. F. F. Marques, R. F. Marques, P. M. Gordo, M. Kajetanowicz, G. Korcyl, L. Lopes, J. Michel, *et al.*, "Towards very high resolution RPC-PET for small animals," *Journal of Instrumentation*, vol. 9, no. 10, p. C10012, 2014.

[55] A. F. Taktak, P. Ganney, and D. Long, *Clinical Engineering: A Handbook for Clinical and Biomedical Engineers*. Academic Press, 2013.

[56] A. Fedorov, R. Beichel, J. Kalpathy-Cramer, J. Finet, J.-C. Fillion-Robin, S. Pujol, C. Bauer, D. Jennings, F. Fennessy, M. Sonka, J. Buatti, S. Aylward, J. V. Miller, S. Pieper, and R. Kikinis, "3D slicer as an image computing platform for the quantitative imaging network," *Magn Reson Imaging*, vol. 30, pp. 1323–41, Nov 2012.

[57] A. M. Loening and S. S. Gambhir, "AMIDE: a free software tool for multimodality medical image analysis," *Mol Imaging*, vol. 2, pp. 131–7, Jul 2003.

Appendices

A

Appendix A

A.1 Source code

```
PRO xget_rectangle_mask, _v_pet, getval=getval, group=group, zoom_factor=_zoom_factor
COMMON tutorial,win,x,y, v_pet, szpet, mask_rect, zoom_factor

  v_pet         = _v_pet
  szpet         = size(v_pet, /dim)
  zoom_factor   = _zoom_factor

  IF N_ELEMENTS(Group) EQ 0 THEN GROUP=0

  base0 = widget_base(GROUP_LEADER=Group, title= 'Select mouse region',/column, /modal)
  base1 = widget_base(base0, /row)
  base2 = widget_base(base0, /row)
  w = widget_draw   (base0, uvalue='w1', xsize=szpet[0]*zoom_factor, ysize=szpet[1]*zoom_factor, /button_events, /MOTION_EVENTS)
  i = widget_button (base0, uvalue='q' , value='Done')

  widget_control, base0, /realize
  widget_control, w, get_value=win

  wset,win
  tvscl, congrid(max(v_pet, dim=3), szpet[0]*zoom_factor, szpet[1]*zoom_factor)

  xmanager, 'tutorial', base0;, /no_block

  minx = mask_rect.first_x < mask_rect.second_x
  maxx = mask_rect.first_x > mask_rect.second_x
  miny = mask_rect.first_y < mask_rect.second_y
  maxy = mask_rect.first_y > mask_rect.second_y
  getval = {first_x :minx, $
            second_x:maxx, $
            first_y :miny, $
            second_y:maxy }
END
```

Figure A.1: Source code of the *widget* designed to isolate fiducial markers selecting the body of the mice by sketching a rectangle surrounding it.

```
function get_threshold, img, nmarkers
  maximg          = float(max(img))
  minimg          = float(min(img))
  fThresholdFound = 0
  nsteps          = 1000.
  offset          = 0;1300.
  stepsize        = (maximg-(minimg+offset))/float(nsteps)
  min_reg_pixels  = 10
  max_reg_pixels  = n_elements(img)/4.
  for j=minimg+offset, maximg,stepsize  do begin
    thresh    = j
    imgaux    = img GT thresh
    lbl_reg   = label_region(imgaux, /ULONG)
    nregions  = max(lbl_reg)
    if nregions EQ nmarkers and fThresholdFound EQ 0 then begin
      h         = histogram(lbl_reg, locations=loc)
      w         = where((h[1:*] GE min_reg_pixels) AND (h[1:*] LE max_reg_pixels), count)
      if count EQ nmarkers then begin
        print, "Region sizes: ", h[1:*]
        min_thresh = j
        fThresholdFound = 1
        print, "Threshold min: ", min_thresh
      endif
    endif
    if nregions NE nmarkers and fThresholdFound EQ 1 then begin
      max_thresh = j-1
      print, "Threshold max: ", max_thresh
      j=maximg
    endif
  endfor
  if n_elements(max_thresh) EQ 0 then max_thresh = maximg
  thresh = (min_thresh + max_thresh)/2.
return, {min_thresh:min_thresh, max_thresh:max_thresh}
```

Figure A.2: Function implemented to bound the threshold by finding maximum and minimum intensity values in which is possible to identify five distinguishable regions.

```
if n_elements(mrifile) EQ 0 then tmp = readmri(/use_default) else tmp = readmri(mrifile)
v_mri  = tmp.vol
sz_mri = float(size(v_mri, /dim))
sx = sz_mri[0]
sy = sz_mri[1]
sz = sz_mri[2]
print, sx, sy, sz
vmri2 = smooth(v_mri,3)
vmri2[mri_mask_rect.first_x:mri_mask_rect.second_x, mri_mask_rect.first_y:mri_mask_rect.second_y,*]=0
vmri3 = vmri2 GT thresh_mri
vlbl = label_region(vmri3)
nregions = max(vlbl)
print, "Number of regions: ", nregions
cenmri = fltarr(3,5)
for i=1, nregions do begin
  w = where(vlbl EQ i, count)
  if count gt 0 then begin
    x = w MOD (sx*sy)
    x = x MOD sx
    y = w MOD (sx*sy)
    y = y / sx
    z = w / (sx*sy)
    cenmri[0,i-1] = mean(x)
    cenmri[1,i-1] = mean(y)
    cenmri[2,i-1] = mean(z)
  endif
  print, "MRI: Region ", i, ": ", cenmri[0,i-1], cenmri[1,i-1], cenmri[2,i-1]
endfor
```

Figure A.3: Part of the code applied to found the regions corresponding to the fiducial markers, their location, and the coordinates of their centroids.

```
ftol = 1.0e-8

; Define the starting point:
P = [3.d, 3.d, 0.5d, -100.d, -100.d, -10.d]
;P = double([1.d, 1.d, 1.d, -0.d, 0.d, -0.d])

; Define the starting directional vectors in column format:
xi = double(TRANSPOSE([ [1.0,0.0,0.0,0.0,0.0,0.0], $
                [0.0,1.0,0.0,0.0,0.0,0.0], $
                [0.0,0.0,1.0,0.0,0.0,0.0], $
                [0.0,0.0,0.0,1.0,0.0,0.0], $
                [0.0,0.0,0.0,0.0,1.0,0.0], $
                [0.0,0.0,0.0,0.0,0.0,1.0]]))

; Minimize the function:
POWELL, P, xi, ftol, fmin, 'distance_min'


for i=0,4 do begin
  print, "Fiducial mark: ", i
  print, "Centroids (MRI)              : ", cenmri[*,i]
  print, "Centroids (PET), after optimiz.: ", $
    cenpet[0,i]*p[0]+p[3], $
    cenpet[1,i]*p[1]+p[4], $
    cenpet[2,i]*p[2]+p[5]
endfor
print, "-------------------------"
print, "Parameters found: ", p
print, "Fmin: ", fmin
print, "-------------------------"
```

Figure A.4: Function implementation of the registration or similarity metric.

```
function distance_min, param
COMMON  name, cenmri, cenpet, v_pet

  r = fltarr(3,5)   ; positions of the 5 fiducial marks seen in PET, after multiplication by a factor scale and displacement
  distance = fltarr(5)

  for i=0, 4 do begin
    r[0,i] = cenpet[0,i]*param[0]+param[3]    ; x
    r[1,i] = cenpet[1,i]*param[1]+param[4]    ; y
    r[2,i] = cenpet[2,i]*param[2]+param[5]    ; z
    distance[i] = sqrt((cenmri[0,i]-r[0,i])^2 + $
                       (cenmri[1,i]-r[1,i])^2 + $
                       (cenmri[2,i]-r[2,i])^2)
  endfor
 chisq = total(distance)
; print, "Param: ", param
; print, "Chisq: ", chisq
 RETURN, chisq
END
```

Figure A.5: Source code implemented to get the transformation offset and scale factors values by minimizing the similarity metric. IDL pre-existent *POWELL()* function was used to perform this operation.

```
; coordinates of xyz grids for PET and for MRI:
x_mri        = min_img_posx_mri  + findgen(sz_mri[0]) * pix_spacing_mri[0]
y_mri        = min_img_posy_mri  + findgen(sz_mri[1]) * pix_spacing_mri[1]
z_mri        = min_img_posz_mri  + findgen(sz_mri[2]) * slice_thickness_mri
x_pet       = min_img_posx_pet + findgen(sz_pet[0])* pix_spacing_pet[0]
y_pet       = min_img_posy_pet + findgen(sz_pet[1])* pix_spacing_pet[1]
z_pet       = min_img_posz_pet + findgen(sz_pet[2])* slice_thickness_pet

; convert coordinates of MRI grid to PET index coordinates (for volume interpolation)
x_pet       =  (findgen(sz_mri[0]) - p[3])/p[0]
y_pet       =  (findgen(sz_mri[1]) - p[4])/p[1]
z_pet       =  (findgen(sz_mri[2]) - p[5])/p[2]

; the PET data, resampled and coregistered so that fiducial marks are aligned
v_pet_interp2  = interpolate(v_pet, x_pet, y_pet, z_pet, /GRID)


vpet3_interp2 = interpolate(vpet3, x_pet, y_pet, z_pet, /GRID)      ; same thing but just with the fiducial marks segmented
```

Figure A.6: Source code implemented to interpolate PET and MRI volumes using the parameters that were obtained with the metric calculation.